

Angle-resolved photoemission spectroscopy study on transition-metal kagome materials

Jiangang Yang(杨鉴刚), Jianwei Huang(黄建伟), Lin Zhao(赵林), and X. J. Zhou(周兴江)

Citation: Chin. Phys. B, 2025, 34 (**4**): 047101. DOI: 10.1088/1674-1056/adb689
Journal homepage: http://cpb.iphy.ac.cn; http://iopscience.iop.org/cpb

What follows is a list of articles you may be interested in

Electronic band structures of topological kagome materials

Man Li(李满), Huan Ma(马欢), Rui Lou(娄睿), and Shancai Wang(王善才)
Chin. Phys. B, 2025, 34 (**1**): 017101. DOI: 10.1088/1674-1056/ad925d

Visualizing the electronic structure of kagome magnet $LuMn_6Sn_6$ by angle-resolved photoemission spectroscopy

Man Li(李满), Qi Wang(王琦), Liqin Zhou(周丽琴), Wenhua Song(宋文华), Huan Ma(马欢), Pengfei Ding(丁鹏飞), Alexander Fedorov, Yaobo Huang(黄耀波), Bernd Büchner, Hechang Lei(雷和畅), Shancai Wang(王善才), and Rui Lou(娄睿)
Chin. Phys. B, 2024, 33 (**11**): 117101. DOI: 10.1088/1674-1056/ad7afe

Coexistence of Dirac and Weyl points in non-centrosymmetric semimetal $NbIrTe_4$

Qingxin Liu(刘清馨), Yang Fu(付阳), Pengfei Ding(丁鹏飞), Huan Ma(马欢), Pengjie Guo(郭朋杰), Hechang Lei(雷和畅), and Shancai Wang(王善才)
Chin. Phys. B, 2024, 33 (**4**): 047104. DOI: 10.1088/1674-1056/ad2a79

Angle-resolved photoemission study of NbGeSb with non-symmorphic symmetry

Huan Ma(马欢), Ning Tan(谭宁), Xuchuan Wu(吴徐传), Man Li(李满), Yiyan Wang(王义炎), Hongyan Lu(路洪艳), Tianlong Xia(夏天龙), and Shancai Wang(王善才)
Chin. Phys. B, 2024, 33 (**2**): 027102. DOI: 10.1088/1674-1056/ad0ccf

Band structures of strained kagome lattices

Luting Xu(徐露婷) and Fan Yang(杨帆)
Chin. Phys. B, 2024, 33 (**2**): 027101. DOI: 10.1088/1674-1056/ad0291

TOPICAL REVIEW — Recent progress on kagome metals and superconductors

Angle-resolved photoemission spectroscopy study on transition-metal kagome materials

Jiangang Yang(杨鉴刚)[1,2], Jianwei Huang(黄建伟)[1], Lin Zhao(赵林)[1,2,3,†], and X. J. Zhou(周兴江)[1,2,3,‡]

[1] *Beijing National Laboratory for Condensed Matter Physics, Institute of Physics, Chinese Academy of Sciences, Beijing* 100190, *China*
[2] *School of Physical Sciences, University of Chinese Academy of Sciences, Beijing* 100049, *China*
[3] *Songshan Lake Materials Laboratory, Dongguan* 523808, *China*

(Received 19 December 2024; revised manuscript received 11 February 2025; accepted manuscript online 17 February 2025)

Angle-resolved photoemission spectroscopy (ARPES) has become a cornerstone technique for elucidating the electronic structures of emergent quantum materials. Among these, kagome materials — distinguished by their two-dimensional lattice of corner-sharing triangles — provide a fertile ground for investigating exotic quantum phenomena, driven by geometric frustration, electronic correlation, and topology. In this review, we present an overview of recent ARPES studies on transition-metal kagome materials. We first outline the fundamental features of their electronic structures, including van Hove singularities, Dirac points, and flat bands, and discuss the novel quantum states that arise from many-body interactions within the kagome lattice. We then highlight key ARPES investigations into these unique electronic structures, detailing their manifestation and associated quantum states in representative kagome materials. Finally, we offer a forward-looking perspective on the potential of ARPES to uncover new quantum phenomena and its broader implications for the study of underlying physics in kagome materials.

Keywords: kagome materials, angle-resolved photoemission spectroscopy, electron correlation, electronic topology

PACS: 71.20.–b, 79.60.–i

DOI: 10.1088/1674-1056/adb689 **CSTR:** 32038.14.CPB.adb689

1. Introduction

In condensed matter systems, the macroscopic properties of materials are governed by the microscopic dynamics of various degrees of freedom under the principles of quantum mechanics. Many physical states and phases, including metallic and insulating behaviors, as well as conventional superconductivity, can be understood within the framework of nearly free electrons and the Landau paradigm. However, it was later realized that strong correlation effects and electronic topology must also be considered to fully capture the rich diversity of exotic quantum states and phases in condensed matter systems. Recently, the investigation of emergent quantum states intertwined with electron correlation and electronic topology has become a forefront topic in condensed matter physics. Transition-metal kagome materials, in particular, offer a fertile ground for exploring novel quantum states and have thus attracted significant research interest in recent years.[1,2] Early studies on these materials focused on quantum spin liquid, exploiting the geometric frustration inherent to the kagome lattice.[3,4] More recently, from an electronic perspective, it has been recognized that the kagome lattice also provides an ideal platform for exploring exotic topological and correlated electronic phases, which arise from the interplay between the geometrically frustrated lattice and the charge degrees of freedom[5–9] [Figs. 1(a)–1(j)].

Angle-resolved photoemission spectroscopy (ARPES) plays a pivotal role in investigating the electronic structure of materials in condensed matter physics.[10] By directly mapping the electronic structure in momentum space, ARPES offers unprecedented insight into the fundamental properties of materials. Thanks to advances in electron optics, laser technology, and cryogenics, ARPES is now capable of revealing the electronic structure with spin, spatial, and temporal resolution under extreme conditions such as strain, low temperatures, and magnetic fields.[11] In this review, we present recent progress in ARPES studies of various kagome systems. We begin by introducing the basic physical principles of kagome electrons and providing an overview of the different classes of kagome materials and their associated physical properties. We then examine the fascinating phenomena associated with the van Hove singularity (vHS)-induced topological charge order in kagome materials. Next, we discuss the emergence of Dirac points and related topological states under spin–orbit coupling, with a focus on kagome Chern magnets and kagome Weyl semimetals. We also address the strongly correlated states driven by flat bands, topological flat bands in the kagome lattice and three-dimensional flat bands in the pyrochlore lattice. Finally, we offer perspectives on future directions for research in kagome materials.

[†]Corresponding author. E-mail: LZhao@iphy.ac.cn
[‡]Corresponding author. E-mail: XJZhou@iphy.ac.cn

© 2025 Chinese Physical Society and IOP Publishing Ltd. All rights, including for text and data mining, AI training, and similar technologies, are reserved.

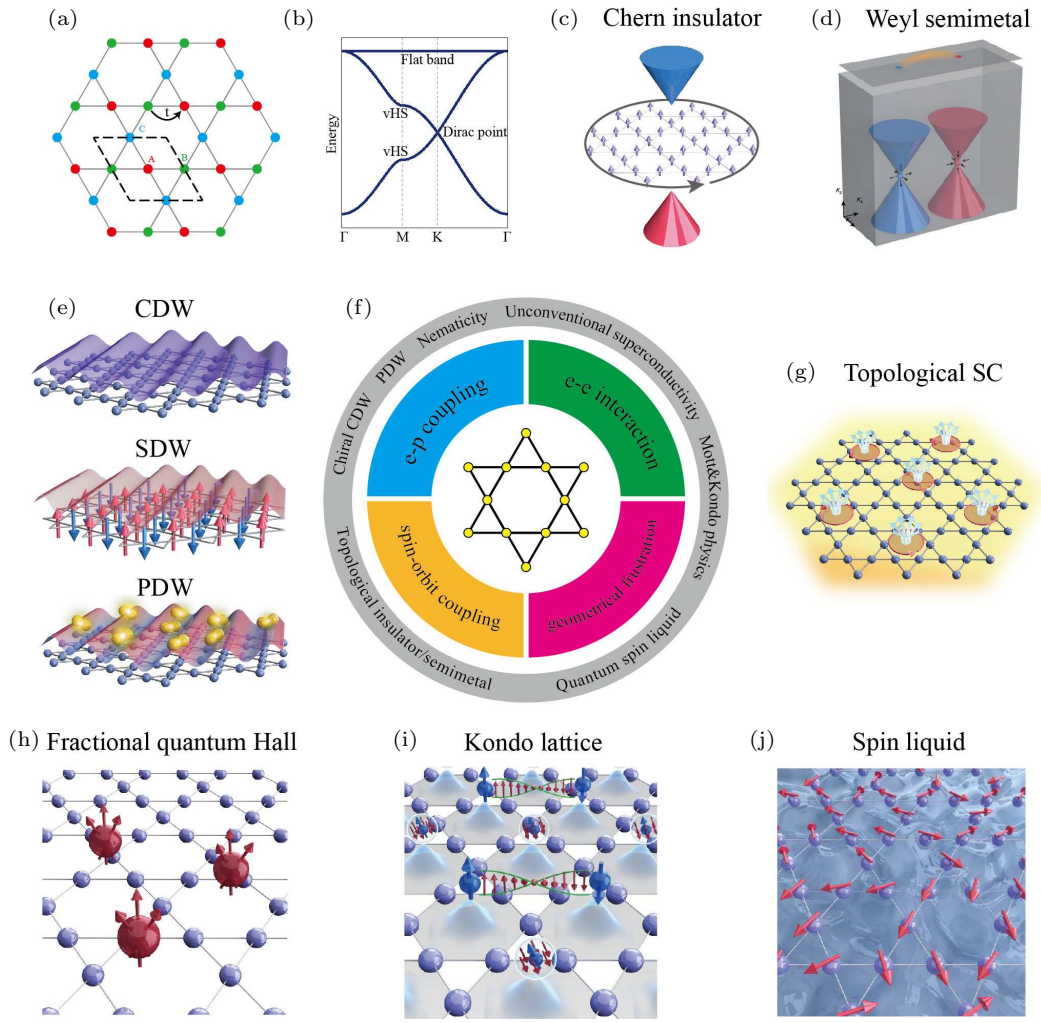


Fig. 1. Characteristic electronic structure and exotic quantum states in kagome lattice. (a) Schematic illustration of tight-binding model in kagome lattice with three inequivalent sites (A, B and C) in the unit cell. The nearest-neighbor hopping t is marked by the arrow. (b) Band structure of kagome tight-binding model. (c) Chern insulator in kagome lattice, the black arrow represents the topological edge state. (d) Weyl fermions in the momentum space. The arrows represent the direction of Berry curvature. (e) Charge density wave (CDW), spin density wave (SDW) and pairing density wave (PDW) in kagome lattice. (f) Exotic quantum phenomena and underlying physics in kagome materials. (g) Topological superconductivity (SC) in kagome lattice. The edge state (red arrow) will emerge at the boundaries of magnetic vortex. (h) Illustration of fractional Chern insulator or fractional quantum Hall effect in kagome lattice. (i) Kondo lattice derived from flat band in kagome lattice. Flat band originated from the localized state in the central hexagon of kagome lattice participates in the formation of Kondo singlet or RKKY interaction. (j) Quantum spin liquid phase in kagome lattice.

2. Physical concept in kagome lattice

The electronic characteristics of a kagome lattice can be well understood with a spinless tight-binding model. There are three sites from inequivalent sublattices, namely, A, B and C in the unit cell of the kagome lattice as shown in Fig. 1(a). Taking into account only the nearest-neighbor (NN) hopping and one isotropic s-orbital, the tight-binding Hamiltonian can be written as

$$H = -t\sum_{ij} c^{\dagger}_{i\alpha} c_{j\beta} + \text{H.c.},$$

where t represents the nearest-neighbor hopping parameter, α and β represent the sublattice indexes. After Fourier transformation, we can write the Hamiltonian in the momentum space as $H = \Sigma_{\boldsymbol{k}} \Psi^{\dagger}_{\boldsymbol{k}} \mathcal{H}_{\boldsymbol{k}} \Psi_{\boldsymbol{k}}$ with $\Psi_{\boldsymbol{k}} = (c_{\mathrm{A}\boldsymbol{k}}, c_{\mathrm{B}\boldsymbol{k}}, c_{\mathrm{C}\boldsymbol{k}})^{\mathrm{T}}$ and

$$\mathcal{H}_{\boldsymbol{k}} = \begin{pmatrix} 0 & 2t\cos(\frac{k\cdot a_1}{2}) & 2t\cos(\frac{k\cdot a_2}{2}) \\ 2t\cos(\frac{k\cdot a_1}{2}) & 0 & 2t\cos(\frac{k\cdot (a_1+a_2)}{2}) \\ 2t\cos(\frac{k\cdot a_2}{2}) & 2t\cos(\frac{k\cdot (a_1+a_2)}{2}) & 0 \end{pmatrix},$$

where t, a_1, a_2 and k represent the NN hopping parameter, lattice vectors and wave vector of reciprocal space, respectively. This 3×3 matrix has three eigenstates which represent three different bands in momentum space including one non-dispersive band $E_1 = -2t$ and two dispersive bands $E_{2,3} = t[1 \pm \sqrt{4(\cos^2(\frac{k\cdot a_1}{2}) + \cos^2(\frac{k\cdot a_2}{2}) + (\cos^2(\frac{k\cdot a_1+a_2}{2}))}]$ as plotted in Fig. 1(b). Therefore, the basic kagome electronic structures consist of a flat band originating from destructive interference effect in line graph lattice,[12–14] a Dirac point and a

pair of vHSs [Fig. 1(b)]. Although the above analysis is based on an isotropic s orbital, this can be easily generalized to other orbitals.[15]

When considering the interactions and couplings between various degrees of freedom, these electronic features provide a fertile ground for the emergence of multiple exotic quantum states [Fig. 1(f)]. Upon including spin–orbit coupling as

$$H_{\mathrm{SOC}} = \mathrm{i}\lambda \sum_{ij} \hat{\boldsymbol{d}}_{ij} \cdot \boldsymbol{\sigma}_{\alpha\beta} \hat{c}^{+}_{i\alpha} \hat{c}_{j\beta},$$

Table 1. Category of transition-metal kagome materials.

Materials	Energy of typical electronic features			Physical property				
	Flat band	vHS	Dirac point	Magnetism	Supercon−ductivity	Correlation	Topology	Ordering
FeSn	−0.23 eV[116]		−0.3 eV[116]	AFM ($T_N \approx 365$ K)[117]		Mass enhancement[118]		Charge order[119]
CoSn	−0.27 eV[15,85]		−0.57 eV[15,85]	PM[15], SG (Fe-doped)[120]				
FeGe		~E_F[56,60]	−0.06 eV, −0.2 eV and −0.6 eV[56, 60]	AFM ($T_N \approx 410$ K)/ ($T_{Canting} \approx 60$ K)[56]		Mass enhancement[121]		CDW ($T_{cdw} \approx$ 100K)[56]
Fe_3Sn_2	−0.2 eV[122]		−0.07 eV and −0.12 eV[16]	FM[16]		Strange metal behaviour[63]	IAHE[16], skyrmion[123]	
Mn_3Sn			slightly above the E_F[24]	AFM ($T_N \approx 420$ K)[23, 24]			IAHE, WSM[23, 24]	
Ni_3In	~E_F[36]					Strange metal behaviour[36]		
RMn_6Sn_6	−0.4 eV and ~E_F (R = Y, Lu)[66, 124]	−0.04 eV (R = Y, Lu)[66, 124]	−0.05 eV (R = Y, Lu)[66, 124]	FM (R = Tb, Dy, Ho, Er, Li, Mg, Ca); AFM (R = Y, Sc, Lu, Tm, Er)[125-129]			IAHE, Chern phase (R = Gd−Ho, Li)[65,129,130]	
RMn_6Ge_6				FM (R = Nd, Sm) AFM (R = Dy−Yb, Sc, Y, Lu, Gd)[131, 132]				
RFe_6Sn_6				AFM (R = Y, Gd, Tb, Dy, Ho, Er, Tm)[133]				
RFe_6Ge_6				AFM (R = Sc, Lu, Ti, Zr, Hf and Nb)[132, 134]				
RV_6Sn_6 (R = Gd, Ho, Sc)	−1 eV[92,135,136]	E_F[92,135,136]	−0.4 eV[92,135,136]	PM (R = Sc)[137, 138]				CDW (R = Sc; $T_{cdw} \approx 92$ K)[138]
AV_3Sb_5 (A = K, Rb, Cs)	−1.1 eV[139]	E_F[45,46,52,53,140-142]	−0.25 eV[45,46,52,53,140-142]		SC (T_c: 0.9−3 K)[43]		TCO & IAHE[31,44,143], TSC[27,28]	CDW[30], PDW[32], nematicity[33]
ATi_3Bi_5 (A = K, Rb, Cs)	−0.24 eV[88,90,91]	above the E_F[144]	−0.2 eV[88, 91]		SC (A = Cs; $T_c \approx 4.8$ K)[87]			Nematicity[89]
ACr_3Sb_5	~E_F[145-147]			AFM SDW at ambient pressure[148]	SC under pressure[148]			CDW, SDW[148]
AV_6Sb_6			~E_F[38]				DSM[149]	
ACr_6Sb_6	~E_F[38]			AFM[38]		Kondo physics[38]		
RTi_3Bi_4	−0.4 ~ −0.8 eV[150,151]	0 ~ −0.5 eV[150,152,153]	~E_F[150,152]	AFM (R = Ce, Gd), FM (R = Nd, Sm, Eu), NM (R = La, Yb), SG (R = Pr)[105, 154]			DSM[150,152,153], TI[153]	
RT_3X_2 (T = Ru,Ir,Rh; X = B,Si,Ga)					SC in $LaRu_3Si_2$ ($T_c \approx 7.8$ K), $LaIr_3Ga_2$ ($T_c \approx 5.2$ K), YRu_3Si_2 ($T_c \approx 3$ K), $LaRh_3B_2$ ($T_c \approx 2.6$ K)[100-102,155,156]			CDW in $La(Ru_{1-x}Fe_x)_3Si_2$[99]
$Co_3Sn_2S_2$	~E_F[157]		slightly above E_F[68, 69]	FM ($T_c \approx 175$ K)[22]		Mass enhancement[158]	WSM[22,68,69,159]	
Nb_3X_8 (X = Cl, Br, I)	−0.5 ~ −1 eV[35,74,75,81]			PM to NM transition[78, 79]		Mott insulator[35,76]		
$CeRu_2$	−0.5 eV[98]		−1.7 eV[98]	Muti-sets magnetic transition[160, 161]	SC ($T_c \approx 6$ K) order[160, 161]			
CaX_2 (X = Ni, Ru)	0 ~ 0.5 eV[97]		−1.7 eV[97]		SC (X = Ru)[97]			
CuV_2S_4	~E_F[37]					Strange metal behaviour[37]		CDW[37]

vHS, van Hove singularity; AFM, antiferromagnetism; FM, ferromagnetism; PM, paramagnetism; NM, nonmagnetism; SG, spin glass; SC, superconductivity; CDW, charge density wave; PDW, pair density wave; IAHE, intrinsic anomalous Hall effect; TSC, topological superconductivity; TCO, topological charge order; DSM, Dirac semimetal; WSM, Weyl semimetal; TI, topological insulator.

where λ is the spin–orbit coupling strength, $\boldsymbol{d}_{ij}$ is the unit vector depending on the type of SOC, and $\boldsymbol{\sigma}$ is the Pauli matrices vector. The inclusion of spin–orbit coupling opens spin-Chern gaps at the Dirac point as well as at the intersection of the flat band and the quadratic band. At these momentum points, strong spin Berry curvature is generated, driving the system into a $\mathbb{Z}_2$ topological phase with robust edge states.[5] Introducing magnetization breaks time-reversal symmetry, lifting the Kramers degeneracy. In this case, the gap transforms into a Chern gap, inducing large Berry curvature and driving the system into a Chern insulator with chiral edge states. Tuning the chemical potential near the gap can induce the anomalous Hall effect,[16] the quantum anomalous Hall effect [Fig. 1(c)],[17–19] and potentially the fractional quantum anomalous Hall state [Fig. 1(h)].[6,20] In a stacked magnetic kagome lattice with strong interlayer coupling, the Chern gap closes at specific momentum points along k_z, appearing in pairs, and giving rise to the formation of Weyl fermions [Fig. 1(d)].[21–24]

The vHS and flat band fillings are favorable for electron correlation, dominating the ground state in the kagome lattice.[7,8,25,26] When considering Hubbard-like interaction

$$H_{\text{int}} = U\sum_i n_{i,\uparrow}n_{i,\downarrow} + V\sum_{i,j,\sigma,\sigma'} n_{i,\sigma}n_{j,\sigma'},$$

where the first term is the local Hubbard interaction scaled by U while the second term is the long-range Hubbard interaction scaled by V. With the van Hove filling, a large density of states (DOS) can lead to strong Fermi surface nesting effects. It is important to note, however, that the local Hubbard interaction U is diagonal in the sublattice space, which introduces a sublattice interference effect that can modify the nesting vector.[7] In contrast, long-range interactions V are not diagonal in the sublattice space, and depending on orbital fillings and Fermi surface topologies, these interactions give rise to a variety of exotic Fermi surface instabilities, including unconventional superconductivity (USC),[27,28] charge density wave (CDW) [Fig. 1(e)],[29–31] pair density wave (PDW) [Fig. 1(e)],[32] and electronic nematicity.[33] These unconventional phases, driven by the condensation of particle—hole or particle–particle pairs, can exhibit nonzero orbital angular momentum and even chirality, resulting in a topologically nontrivial order parameter [Fig. 1(g)] and the breaking of time-reversal symmetry.[28,30,34] With the flat-band filling, strongly correlated phases such as Mott insulators, Kondo lattice states [Fig. 1(i)] and non-Fermi liquid behavior may emerge.[35–38] Unlike the strong electron correlation arising from localized orbital wave functions, the correlation induced by geometric frustration carries nontrivial electronic geometry, providing a platform for the interplay between electron correlation and electronic topology.[39]

In real materials, thousands of known compounds feature a kagome lattice structure. However, those in which the kagome network is formed by transition metal atoms are of particular interest due to the interplay between topology

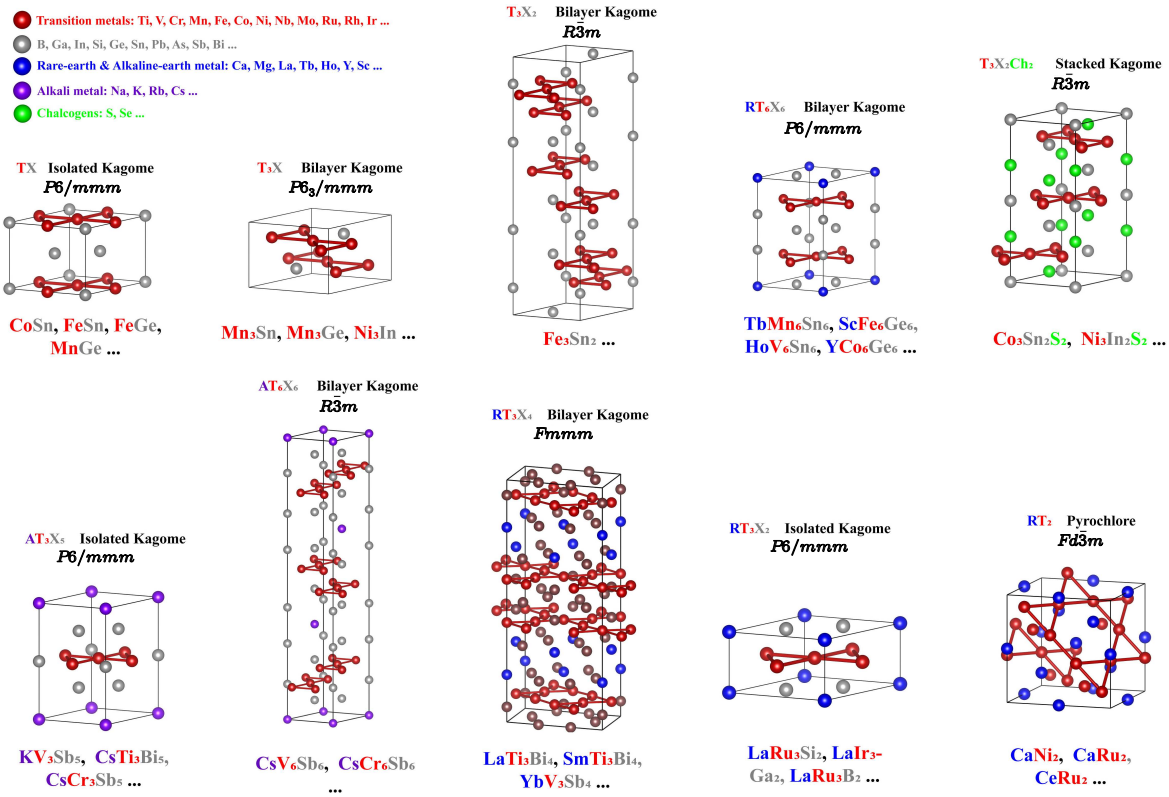


Fig. 2. Crystal structures and chemical compositions of various classic transition metal kagome materials.

and electron correlations. Despite the fascinating physics discussed above, it should be noted that the typical kagome band structures are often distorted or even destroyed by strong interlayer interactions and orbital hybridization.[40] Some general principles have been summarized for identifying ideal kagome compounds based on their chemical composition.[40] These rules help narrow down the search for ideal kagome compounds. We believe that an overview of these typical ideal kagome compounds is essential for guiding future research. As shown in Fig. 2, we summarize several prominent transition metal kagome families and list their corresponding electronic structures and related quantum states in Table 1.

3. Angle-resolved photoemission spectroscopy

ARPES is a powerful experimental technique for studying the electronic structure of materials. By irradiating a sample with high-energy photons, typically from a synchrotron or laser source, ARPES measures the kinetic energy and emission angles of the ejected electrons. This information provides direct insight into the material's band structure, including the energy–momentum dispersion relations, Fermi surface topology, and many-body interactions. Based on the energy conservation law in the photoemission process, the kinetic energy of photoemission $E_{\rm kin}$ can be expressed as

$$E_{\rm kin} = h\nu - \phi - E_{\rm B},$$

where $h\nu$ is the energy of the incident photon, ϕ is the work function of the material and $E_{\rm B}$ is the binding energy of the electron in the material. Considering momentum conservation in the parallel direction of the surface, the parallel momentum $k_{\parallel}$ can be expressed as

$$k_{\parallel} = \sqrt{2m_{\rm e}E_{\rm kin}/\hbar^2}\sin\theta,$$

where $m_{\rm e}$ is the mass of the electron and θ is the emission angle of the ejected electrons. The perpendicular momentum $k_{\perp}$ is not conserved. However, it can be estimated by considering the inner potential V_0

$$k_{\perp} = \hbar^{-1}\sqrt{2m_{\rm e}\left(E_{\rm kin}\cos^2\theta + V_0\right)}.$$

The inner potential V_0 is entirely material-dependent, which implies that by varying the photon energy $h\nu$, different $k_{\perp}$ of the material can be probed.

ARPES measures the distribution of spectral intensity as a function of electron momentum and energy. It is proportional to several factors

$$I(\boldsymbol{k},\omega) \propto |M_{\boldsymbol{k}}|^2 \cdot A(\boldsymbol{k},\omega)\cdot f(\omega,T).$$

Among them, $M_{\boldsymbol{k}}$ is the matrix elements dependent on the initial and final states of the photoelectron, the photon energy, and the polarization of the incident light. Utilizing the matrix element effects can elucidate the orbital characters of the bands.[41] $A(\boldsymbol{k},\omega)$ is the one-particle spectral function. The energy bands can be visually observed from it and quantitative dispersions can be obtained by data fitting. In general, a flat band shows a quite weak dispersion, Dirac cone shows the intersection of two linear energy bands and crosses a van Hove singularity, the curvature of the band is opposite in sign on either side. A comparison between the experimental bands and the band calculation is sometimes necessary to further identify the band feature. An in-depth analysis of it can extract the electron self-energy, thereby providing detailed information on the many-body interaction within the material.[41] $f(\omega,T)$ is the Fermi–Dirac distribution which describes the thermal occupation of electronic states. It limits the ability of ARPES to measure unoccupied states.

In practical research utilizing ARPES on kagome materials, one often encounters numerous intricate issues. Firstly, ARPES is a surface-sensitive detection method, particularly when photons with energies in the range of 10–100 eV are employed. This means that the electronic structure detected typically originates from the sample's surface, necessitating attention to the effects of different cleaved surfaces. For some kagome materials, the electronic structure stemming from the kagome lattice can only be observed within the kagome cleaved surface, which also imposes requirements on the spot size of the beam. Secondly, many kagome materials may exhibit strong interlayer coupling, leading to significant dispersion along the k_z direction. This can result in spectral broadening due to the limitations of k_z-resolution and underscores the need for photon energy-dependent measurements. When studying magnetic kagome materials, photoemission obtained from low-energy photons is often susceptible to the sample's magnetic properties, causing spectral broadening, which is another issue to be mindful of. Currently discovered kagome superconductors typically have superconducting transition temperatures of only a few Kelvins, making the study of their superconducting properties with ARPES challenging. This often requires ultra-high energy resolution and advanced cryogenic techniques.

4. The van Hove singularity and Fermi surface instability

The Fermi surface instability induced by the filling of vHSs leads to the emergence of various quantum ordered states.[7,8,25,26] Meanwhile, the interplay of these quantum ordered phases results in a series of complex yet rich physical phenomena in kagome materials. The emergent quantum state driven by vHSs has been extensively investigated in kagome materials AV_3Sb_5 (A = K, Rb and Cs) and FeGe recently. In

this section, we will discuss how ARPES helps us understand the underlying physical mechanisms in these materials.

4.1. Topological kagome superconductor AV_3Sb_5

The AV_3Sb_5 family was first synthesized in 2019,[42] and was later found to host coexistence of superconductivity and CDW transition.[43] The subsequent experiments revealed that an intrinsic anomalous Hall effect is accompanied with the charge order in these systems.[44] Other symmetry breaking orders including PDW and electronic nematicity were also observed in this system.[32,33] These complex orders coexisted with superconductivity are reminiscent of the case in cuprate superconductors. As shown in Fig. 3(a), AV_3Sb_5 crystallizes in the hexagonal structure with space group $P6/mmm$ featuring a perfect V-atoms-constructed kagome lattice. A charge order transition and also the superconductivity were observed in transport measurement [Fig. 3(b)].[43] ARPES revealed four Fermi surface sheets labeled with α, β, γ and δ [Fig. 3(c)] which are consistent with band structure calculation [Fig. 3(d)].[45] The α band is derived from Sb-5p orbitals while the β, γ and δ bands are dominated by V-3d orbitals. Two sets of V-orbital derived vHSs were found close to the Fermi level [Figs. 3(e) and 3(f)].[46] These vHSs result in large density of state at the Fermi level and nesting vector $(\pi,0)$ connecting different vHSs in momentum space [Fig. 4(a)], probably leading to the charge order transition. X-ray scattering and STM study revealed that there is a 2×2 inverse star-of-David charge order below T_{co} = 78–102 K[29,30,47] with rotation-symmetry breaking.[30] Muon spin relaxation revealed that not only translational symmetry but also time reversal symmetry are broken in the charge order state[31] with a large anomalous Hall effect observed under the transition.[44] All these results imply an unconventional CDW instead of a traditional Peierls instability in AV_3Sb_5. A nontrivial chiral flux phase was put forth to understand these phenomena,[34,48,49] which is reminiscent of the loop-current model for the pseudogap phase in cuprates[50] and the Haldane model in graphene.[51]

As shown in Figs. 4(b) and 4(c), temperature dependent ARPES measurement revealed a strong CDW-induced band renormalization at low temperature in CsV_3Sb_5[52] and also in RbV_3Sb_5[53] and KV_3Sb_5.[45] These band renormalizations gap the electronic state at the Fermi level. Based on high-resolution ARPES, an anisotropic CDW gap was captured [Fig. 4(f)]. The Sb-5p orbital derived α band is gapless over the whole Fermi surface while V-orbital derived β, γ and δ bands are gapped with nodes along Γ–K direction.[45] The underlying mechanisms of the CDW order in AV_3Sb_5 are under debate. Besides the unconventional nature of CDW order, the superconductivity order and the role of phonon excitation remain elusive but intriguing. Previous laser-ARPES study revealed that there is intermediate electron–phonon coupling in CsV_3Sb_5 which is able to pair the electrons for superconductivity condensation with a T_c of several Kelvins [Figs. 4(d) and 4(e)].[54] An isotropic superconducting gap was also observed in doped CsV_3Sb_5 based on ultrahigh-resolution-laser ARPES [Figs. 4(g)].[55] The nodeless electron pairing implies a trivial s-wave pairing which is at odds with other experiments.[55] However, it has to be noted that this result can not rule out some nontrivial nodeless gap symmetry such as $d+id$ pairing due to the lack of phase information in APRES measurement.

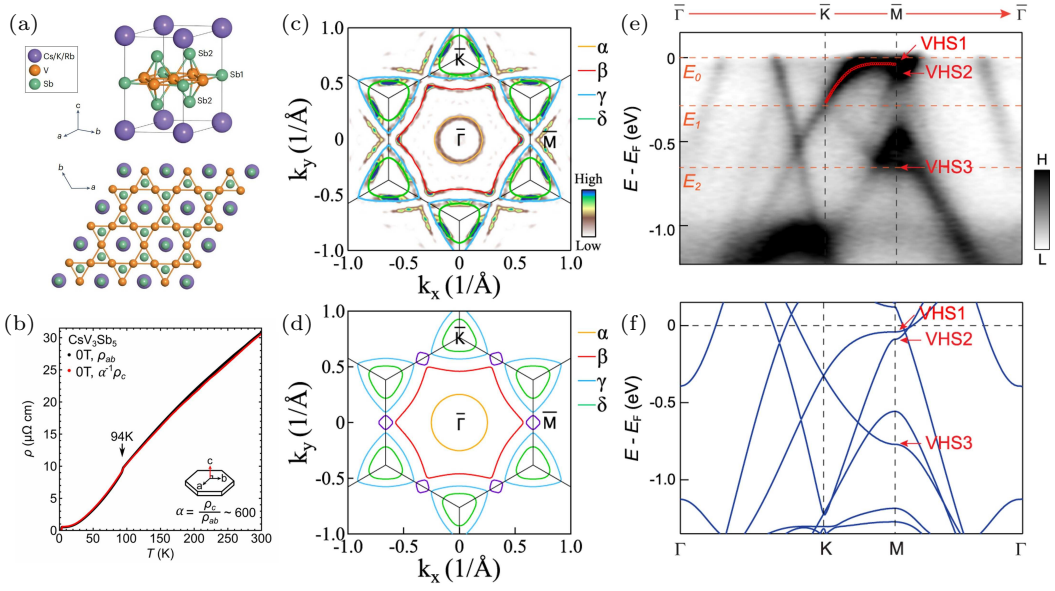


Fig. 3. Crystal and electronic structures of AV_3Sb_5. (a) Crystal structure of AV_3Sb_5. (b) Resistivity measurement of CsV_3Sb_5. The CDW transition is marked by the resistivity anomaly at 94 K. (c) Fermi surface topology of KV_3Sb_5 from ARPES. (d) The calculated Fermi surface of KV_3Sb_5. (e) Experimental band structure along the high symmetry direction of CsV_3Sb_5. (f) Calculated band structure along the high symmetry direction of CsV_3Sb_5. Panel (a) adapted from Ref. [2]. Panel (b) adapted from Ref. [43]. Panels (c) and (d) adapted from Ref. [45]. Panels (e) and (f) adapted from Ref. [46].

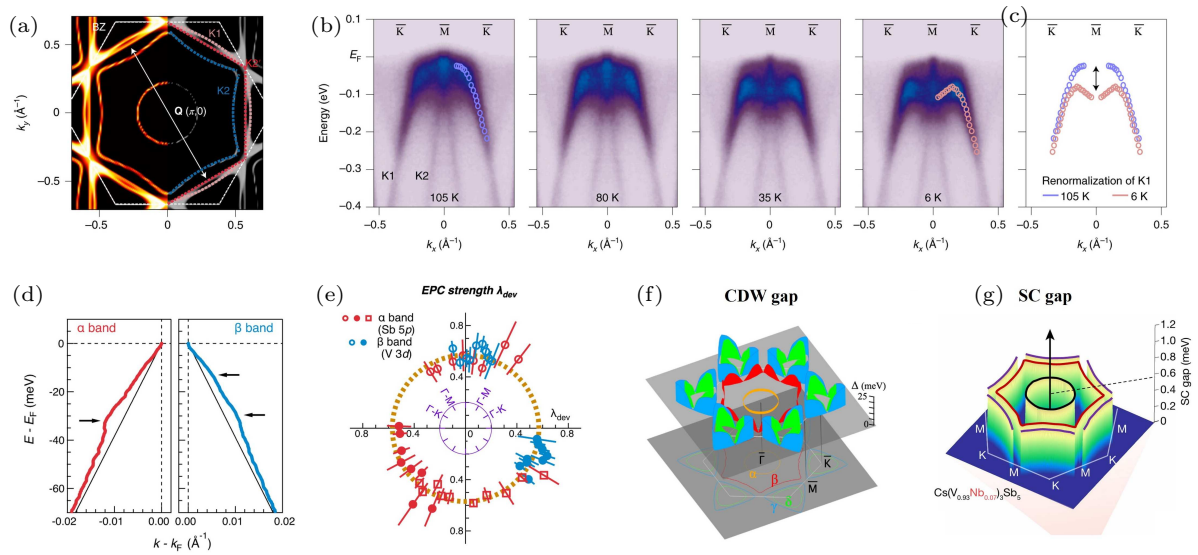


Fig. 4. Band renormalization and energy gap of AV_3Sb_5. (a) Fermi surface of CsV_3Sb_5 and the vHS-derived nesting nature of the 2×2 charge order indicated by the nesting vector (white arrow) . [(b) and (c)] Observation of band renormalization at the vHS across the charge order transition. (d) Evidence of electron–phonon coupling (EPC) in CsV_3Sb_5. The arrows marked the dispersion anomaly due to the coupling. (e) Band- and angle-dependent EPC strength of CsV_3Sb_5 extracted from analysis of self-energy based on ARPES high-resolution measurement. (f) Anisotropic CDW gaps in KV_3Sb_5. (g) Isotropic SC gaps in doped CsV_3Sb_5. Panels (a)–(c) adapted from Ref. [52]. Panels (d) and (e) adapted from Ref. [54]. Panel (f) adapted from Ref. [45]. Panel (g) adapted from Ref. [55].

4.2. Kagome antiferromagnet FeGe

Magnetic kagome lattices provide an excellent platform for investigating the interplay between magnetic correlations and topology.[22,23,56] Among these systems, the kagome antiferromagnet FeGe, featuring a Fe-constructed kagome lattice [Fig. 5(a)], has attracted significant attention due to the coexistence of charge order and magnetism. FeGe, a hexagonal compound, was first synthesized in 1963 and confirmed as an antiferromagnet with a Néel temperature of $T_N \approx 410$ K.[57] Later, magnetic susceptibility measurements revealed a spin-canted structure at lower temperatures.[58] More recently, a combination of susceptibility, transport, scattering, scanning tunneling microscopy (STM), and ARPES has confirmed the antiferromagnetic transition at $T_N \approx 410$ K, the spin-canted antiferromagnetic structure below $T_{canting} \approx 60$ K, and an intriguing $2 \times 2 \times 2$ CDW transition at $T_{CDW} \approx 110$ K, accompanied by an enhancement of the antiferromagnetic moment [Fig. 5(b)].[56] Furthermore, STM studies have revealed the presence of a CDW gap and edge states within the gap, pointing to the nontrivial nature of the charge order, similar to the case of AV_3Sb_5.[59]

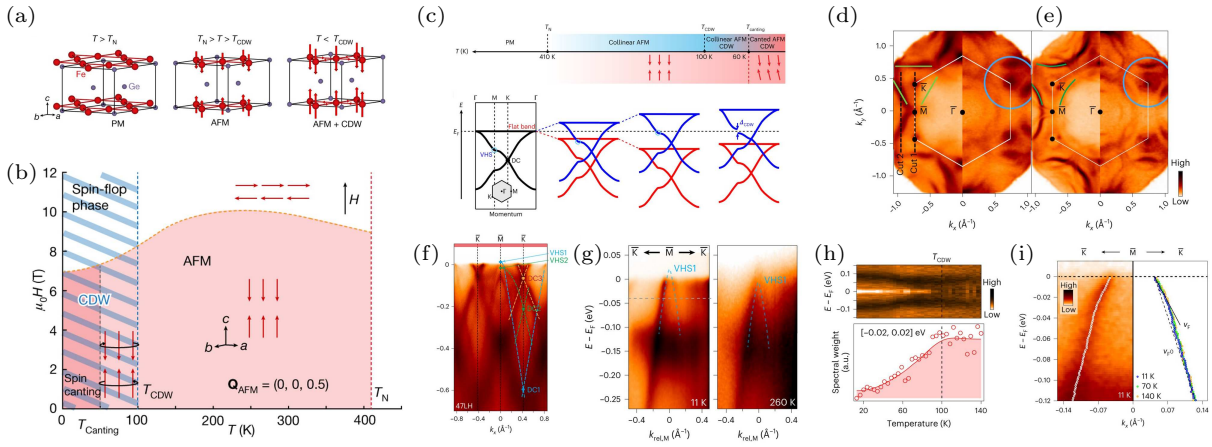


Fig. 5. Crystal structure, electronic structure and phase diagram of FeGe. (a) Schematic illustration of crystal and magnetic structures of FeGe in paramagnetic (PM) phase, antiferromagnetic (AFM) phase and AFM + CDW phase. Enhanced antiferromagnetic moments are shown due to the formation of the CDW state. (b) Temperature–field phase diagram of FeGe. (c) Electronic and magnetic transition and the schematic illustration of AFM-induced band splitting plotted in FeGe, this band splitting shifts the vHS to the Fermi level and helps in the emergence of CDW order. (d) Fermi surface measured at AFM state above the CDW transition. Two vHSs are marked by green and blue lines. (e) Fermi surface measured at low temperature where canted AFM and CDW coexist. (f) Measured band structure along high symmetry direction showing the vHSs and Dirac points near the Fermi level. (g) Observation of the CDW-induced vHS renormalization. (h) Observation of CDW gap extracted from EDC taken at vHS points. (i) Evidence of EPC in FeGe. Panels (a) and (b) adapted from Ref. [56]. Panels (c)–(i) adapted from Ref. [60].

As summarized in Fig. 5(c), the kagome antiferromagnet FeGe hosts a flat band at the Fermi level in the absence of magnetism. Below the Néel transition at $T_N \approx 410$ K, the band splits into two branches due to the onset of antiferromagnetic (AFM) order, causing the vHS to shift to the Fermi level. The CDW order begins to emerge below $T_{CDW} \approx 110$ K. This scenario is supported by temperature-dependent ARPES measurements [Fig. 5(g)]. Figures 5(d) and 5(e) show the Fermi surface at 140 K (above the CDW transition) and 13 K (below the transition), respectively, highlighting the renormalization of the fermiology and band structure at the transition. The two vHSs are dominated by different Fe-3d orbitals, indicating an orbital-selective nature [Fig. 5(f)]. In Fig. 5(h), temperature-dependent energy distribution curves (EDCs) at the vHSs show a significant suppression of spectral weight at the Fermi level, confirming the formation of the CDW gap in FeGe. Additionally, evidence for electron–phonon coupling is provided by high-resolution ARPES [Fig. 5(i)].[60] These similarities between FeGe and AV_3Sb_5 suggest a universality in their underlying CDW mechanism. However, it should be noted that in AV_3Sb_5, electron correlations are expected to be weaker than in FeGe, as evidenced by the band renormalization observed in ARPES measurements compared to density functional theory (DFT) calculations.[52,60] Therefore, a key question remains as to what extent do electron correlations and magnetism contribute to the emergence of charge order in FeGe.[61]

5. Dirac fermions and electronic topology

Inherited from the hexagonal lattice, the kagome lattice features the Dirac points at the Brillouin zone corners. The interplay between these Dirac points and the material's symmetry and interactions often serves as a precursor to the emergence of topological states. For instance, the Dirac points may split or shift in response to interactions like magnetic ordering or spin–orbit coupling, creating exotic topological phases such as topological insulator,[5] Weyl semimetal[21] and anomalous quantum Hall effect.[17,18] In this section, we firstly discuss the ARPES studies on the Chern physics found in kagome magnet Fe_3Sn_2 and RT_6X_6 (R = rare-earth elements, T = Mn, Fe, Co; X = Sn, Ge). Then we discuss the Weyl physics in kagome magnet $Co_3Sn_2S_2$ revealed by ARPES.

5.1. Kagome Chern magnet

Although extensive theoretical studies have provided a broad understanding of the topology in magnetic kagome models, the realization of these non-trivial band structures in specific kagome materials has been slow. In 2011, the kagome magnet Fe_3Sn_2 was discovered to exhibit a large intrinsic anomalous Hall effect, suggesting non-trivial Berry curvature and possible Chern topology in this material.[62] Fe_3Sn_2 possesses an out-of-plane ferromagnetic order with a high Curie temperature ($T_C \approx 640$ K). ARPES studies have revealed two

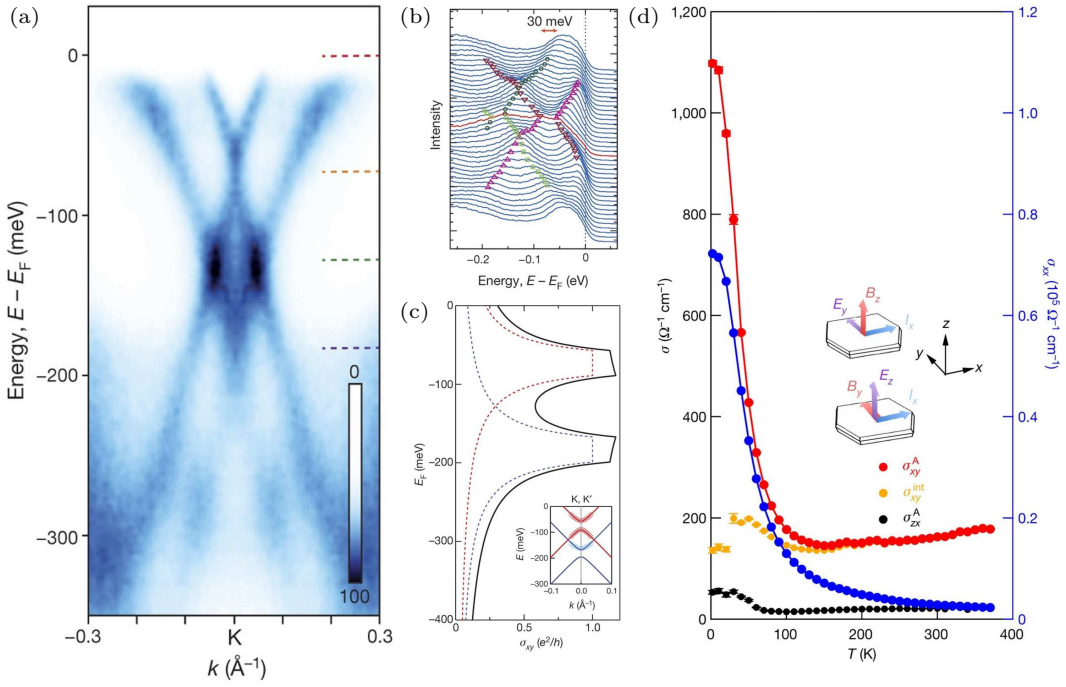


Fig. 6. Massive Dirac fermions and anomalous Hall effect in kagome magnet Fe_3Sn_2. (a) Observation of two massive Dirac fermions in Fe_3Sn_2 by ARPES. (b) EDC stack of (a) showing the gap at the Dirac points. (c) Summary of the correspondence of anomalous Hall conductivity σ_{xy} (black line) as a function of Fermi energy E_F (black solid curve; see text) and the energy position of massive Dirac fermions (blue and red dashed lines). When the Fermi level is set in the gap, the quantum Hall conductance can be observed. (d) Measured anomalous Hall conductivities σ_{xy}^A (red, left axis), σ_{zx}^A (black, left axis), longitudinal conductivity σ_{xx} (blue, right axis) and estimated intrinsic Hall conductivity σ_{xy}^{int} (orange, left axis). All the panels adapted from Ref. [16].

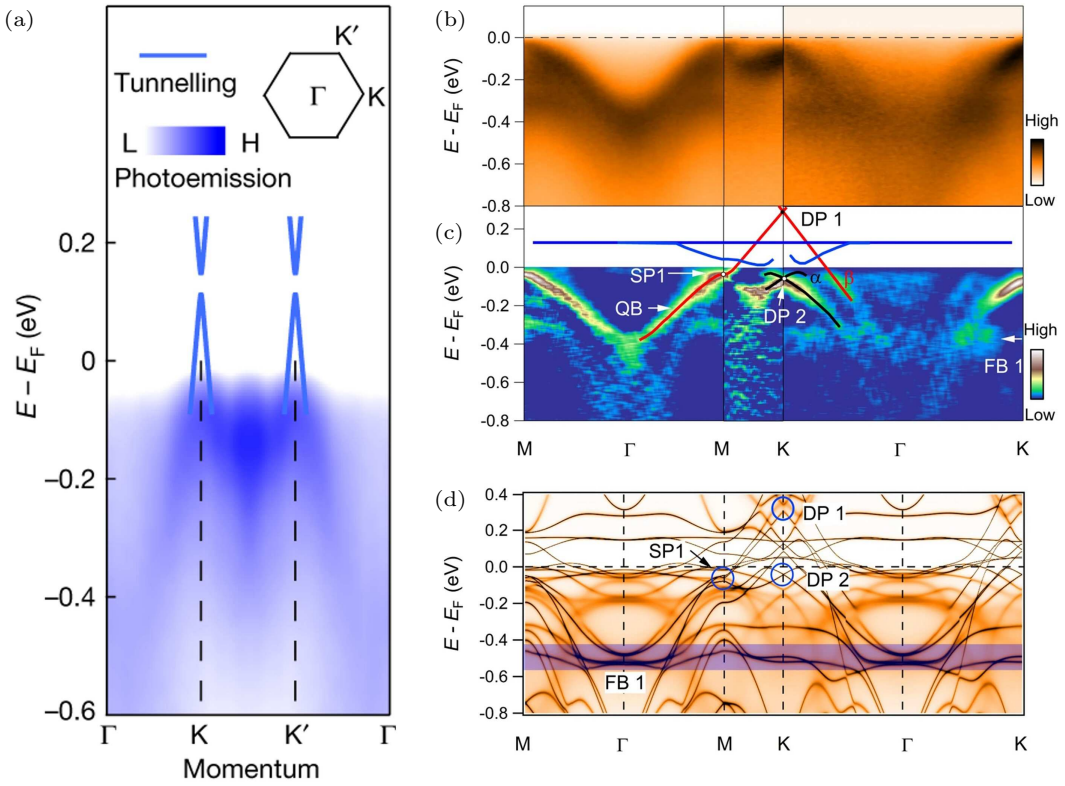


Fig. 7. Massive Dirac fermions in kagome magnet $TbMn_6Sn_6$ and YMn_6Sn_6. (a) Observation of massive Dirac fermion in $TbMn_6Sn_6$ by ARPES. (b) Measured band structure along high symmetry direction of YMn_6Sn_6. (c) Corresponding second derivative plots of (b). A Dirac point and vHSs are close to the Fermi level. (d) DFT + DMFT calculation of band structure along high symmetry direction considering SOC. Panel (a) adapted from Ref. [65]. Panels (b)–(d) adapted from Ref. [66].

Dirac points near the Fermi level, originating from its bilayer kagome lattice structure[16] [Figs. 6(a) and 6(b)]. The spin–orbit coupling transforms these into a pair of massive Dirac fermions. Considering the ferromagnetic nature of Fe_3Sn_2, the intrinsic anomalous Hall effect is believed to arise from the large Berry curvature near the gap. This can be intuitively understood through simple model calculations [Fig. 6(c)], where the magnitude of the anomalous Hall effect depends on the position of the massive Dirac fermions relative to the Fermi level. This intrinsic anomalous Hall conductivity was confirmed by transport measurements [Fig. 6(d)]. It is important to note that Fe_3Sn_2 exhibits a complex magnetic structure at low temperatures, and its ground state may involve the formation of an in-plane antiferromagnetic structure.[16] This antiferromagnetic interaction could disrupt the Chern gap, and as such, there remains ongoing debate regarding its Chern physics. Recently, high-resolution laser-based ARPES studies have revealed strong correlation effects in Fe_3Sn_2, such as non-Fermi liquid behavior, and the emergence of a quasiparticle band due to electron correlations at low temperatures.[63] Additionally, scanning tunneling spectroscopy (STS) studies have detected elusive electron nematicity.[64] These findings suggest that Fe_3Sn_2 is an excellent platform for studying the interplay between Chern topology and electron correlation.

Recently, another family of intermetallic kagome compounds, RT_6X_6 (R = rare earth elements, T = Mn, Fe, Co; X = Sn, Ge), known as the "166" family, has attracted attention in the search for potential kagome Chern magnets. In $TbMn_6Sn_6$, a spin-polarized Dirac cone was observed just above the Fermi level through a combination of ARPES and scanning tunneling microscopy [Fig. 7(a)].[65] Under an applied magnetic field, a large Chern gap opened, and a topological edge state was discovered at the domain boundary.[65] Transport measurements further confirmed the presence of a significant anomalous Hall effect in the system.[65] These findings suggest that $TbMn_6Sn_6$ resides in the Chern insulator phase.[65] Additionally, in another kagome antiferromagnet, YMn_6Sn_6, ARPES studies revealed a pair of spin-polarized massive Dirac fermions near the Fermi level [Figs. 7(b)–7(d)], providing another promising candidate for a Chern insulator.[66]

5.2. Kagome Weyl semimetal

The kagome lattice provides an excellent platform for studying topological insulators and associated Chern physics. Studies have demonstrated that stacking two-dimensional Chern insulators with strong interlayer coupling can lead to the realization of Weyl semimetals.[21] This insight has motivated the search for such exotic topological states in three-dimensional kagome magnets with strong interlayer coupling. $Co_3Sn_2S_2$ has emerged as a promising candidate [Figs. 8(a)–8(g)].

$Co_3Sn_2S_2$ crystallizes in a rhombohedral structure, with

Co_3Sn layers sandwiched between sulfur atoms [Fig. 8(a)]. The magnetic cobalt atoms form an out-of-plane ferromagnetic kagome lattice, where strong S^{2-} ionic bonds facilitate interlayer coupling [Fig. 8(a)]. This material exhibits chiral-anomaly-induced negative magnetoresistance and a giant anomalous Hall effect, both resulting from the enhanced Berry curvature near Weyl points.[22] The Brillouin zone contains six Weyl rings protected by lattice symmetry [Fig. 8(b)]. When spin–orbit coupling (SOC) is included, the topologically protected Weyl nodes persist on these rings, possessing opposite topological charges that generate significant Berry curvature [Fig. 8(c)]. These Weyl nodes, located approximately 60 meV above the Fermi level as predicted by theoretical calculations,[67] were directly observed via ARPES using *in-situ* electron doping with potassium [Figs. 8(f) and 8(g)].[68] Experimentally, the topologically protected surface Fermi arcs connecting two Weyl points were also observed [Fig. 8(d)],[68,69] and photon-energy-dependent ARPES measurements confirmed their two-dimensional nature [Fig. 8(e)].[68] Additionally, temperature-dependent ARPES measurements revealed the annihilation of Weyl fermions during the transition from a ferromagnetic to a paramagnetic state, demonstrating the potential for magnetic manipulation of these topological states for functional applications.[69,70]

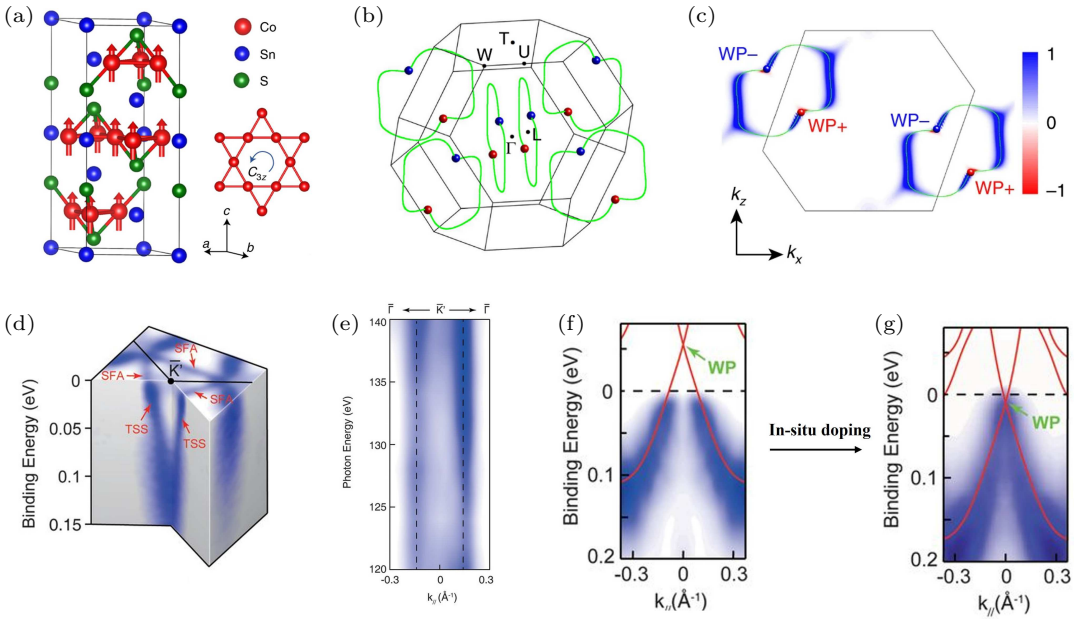


Fig. 8. Weyl fermions and topological surface Fermi arcs in $Co_3Sn_2S_2$. (a) Crystal and magnetic structures of $Co_3Sn_2S_2$. The Co-atoms (red ball) form kagome nets with in-plane ferromagnetism. (b) Nodal rings and the topologically protected Weyl points in the Brillouin zone. (c) Calculated Berry curvature distribution along the nodal ring. (d) Observation of topological surface Fermi arcs. (e) Photon energy dependent ARPES spectral intensity map of the topological surface state. (f) and (g) Observation of Weyl point (WP) after *in-situ* surface doping. Panels (a)–(c) adapted from Ref. [22]. Panels (d)–(g) adapted from Ref. [68].

6. Flat band physics

The electron flat bands stemming from the unique structure of the kagome lattice favor strong electron correlations in the material's physical properties. Similar to the strong electron correlations caused by the localization of electronic wave functions, the kagome flat band also gives rise to a series of strong electron correlation states, including Mott insulators, heavy fermion behavior, unconventional superconductivity, quantum spin liquids, and so on. What's even more exciting is that this quantum destructive interference induced electronic flat bands also host potential electronic topology, thereby giving rise to the concept of topological flat bands and providing an ideal platform for studying correlated topological states of matters.[71] In this section, we discuss the ARPES studies on several kagome flat band families and related exotic physical properties.

6.1. Strongly correlated state with flat band filling

Mott insulator, as a classical manifestation of strongly correlated electrons, successfully explains the abnormal insulating behavior observed in transition metal oxides.[72] Doping a Mott insulator is also regarded as a crucial approach for understanding high-temperature superconductivity.[73] Recently, this strongly correlated electronic state has been proposed in the kagome material family Nb_3X_8 (X = Cl, Br, I) [Figs. 9(a)–9(h)].[35,74–77] These compounds crystallize in a van der Waals-like structure [Fig. 9(a)] with a breathing kagome net formed by Nb atoms [Figs. 9(b) and 9(c)]. At low temperatures, bulk Nb_3X_8 exhibits a non-magnetic β-phase. As the temperature increases, these materials undergo a first-order phase transition, from the low-temperature non-magnetic β-phase to the high-temperature paramagnetic α-phase.[78,79] Transport measurements show that Nb_3X_8 ex-

hibits strong insulating behavior, which contradicts the metallic behavior predicted by first-principles calculations,[35,80] suggesting the presence of electron correlation.

ARPES studies of Nb_3Cl_8[35,74] [Fig. 9(d)], Nb_3I_8[75] [Fig. 9(g)], and Nb_3Br_8[75] have revealed the existence of electronic flat bands and energy gaps near the Fermi level. These experimental observations align with theoretical calculations that incorporate strong Hubbard interactions [Figs. 9(e) and 9(h)]. From this perspective, the insulating behavior of Nb_3X_8 can be understood within the framework of Mott physics[48,76,77] [Fig. 9(f)]. A partially filled flat band favors Mott insulating behavior, and its hybridization with other itinerant bands can also give rise to a range of strongly correlated phenomena. One such example is Kondo physics, which has been extensively studied in f-electron materials in terms of quantum criticality, heavy fermions, strange metallicity, and magnetism.[82] Recently, possible Kondo physics has been discovered in several kagome compounds, where the kagome flat band is thought to play the role of localized magnetic moments instead of f-electrons.

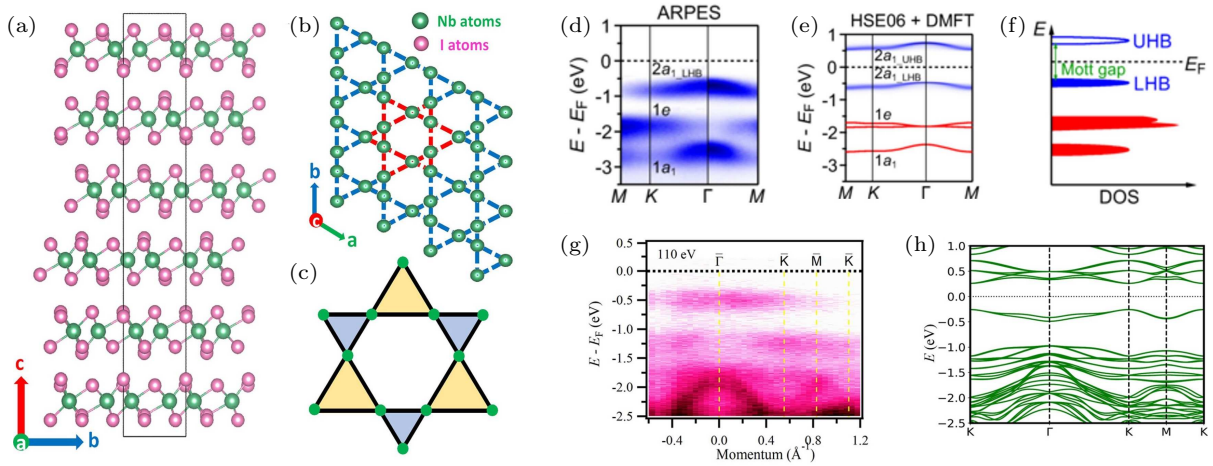


Fig. 9. Mottness in kagome van der Waals Nb_3X_8 (X = Cl, Br and I). (a) Crystal structure of Nb_3I_8. The structures of Nb_3Cl_8 and Nb_3Br_8 are the same with Nb_3I_8 where the I atoms are replaced by Cl or Br. (b) Nb atoms forming a breathing kagome lattice as schematically illustrated in panel (c). (d) Measured band structure along high symmetry direction of Nb_3Cl_8. (e) Calculated band structure of Nb_3Cl_8 along high symmetry direction when considering the on-site Coulomb interaction. The result perfectly reproduces the ARPES data in panel (d). (f) Schematic illustration of Mott insulator state of Nb_3Cl_8. (g) Measured band structure along high symmetry direction of Nb_3I_8. (h) Calculated band structure of Nb_3I_8 along high symmetry direction when considering the on-site Coulomb interaction which perfectly reproduces the ARPES data in panel (g). Panels (a)–(c) adapted from Ref. [75]. Panels (d)–(e) adapted from Ref. [35]. Panels (g) and (h) adapted from Ref. [75].

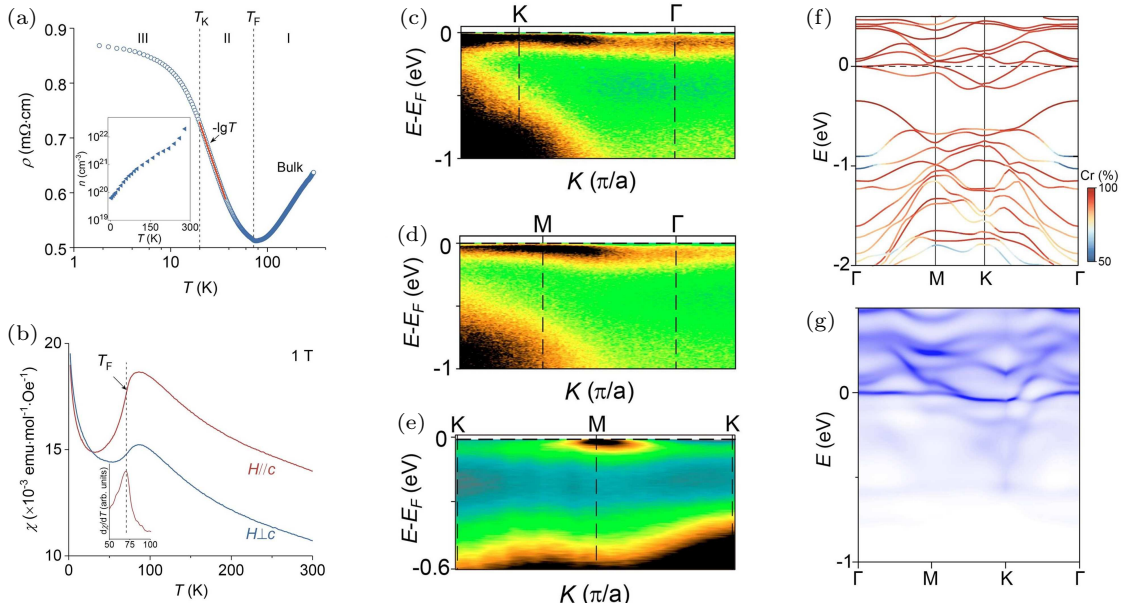


Fig. 10. Manifestation of Kondo physics in kagome materials $CsCr_6Sb_6$. (a) Temperature-dependent resistance of $CsCr_6Sb_6$. Two resistivity anomalies are observed (T_K and T_F). Inset shows the measured carrier density. (b) Temperature-dependent magnetic susceptibility χ of $CsCr_6Sb_6$ along and perpendicular to the c-axis. Inset is the $d\chi/dT$ curve. (c)–(e) Measured band structure along the high symmetry direction of $CsCr_6Sb_6$. A flat band is observed to be located at the Fermi level. (f) Calculated band structure of $CsCr_6Sb_6$ by density functional theory (DFT). Color represents the spectral weight percentage of Cr relative to the summation of Cr and Sb content. (g) Calculated band structure of $CsCr_6Sb_6$ by dynamical mean field theory (DMFT) considering $U = 1.8$ eV. All the panels adapted from Ref. [38].

In the van der Waals kagome antiferromagnet $CsCr_6Sb_6$, manifestation of Kondo physics has been observed.[38] $CsCr_6Sb_6$ crystallizes in the hexagonal space group R-3m, consisting of a double-layer Cr-kagome network [Fig. 2]. Transport measurements [Fig. 10(a)] of bulk $CsCr_6Sb_6$ reveal metallic behavior at high temperatures, with a significant upturn below $T_F \approx 72$ K, where canonical $-\ln T$ Kondo scattering like behavior begins to emerge. As the temperature continues to decrease, the resistivity deviates from the $-\ln T$ dependence and saturates at T_K, representing the formation of Kondo singlet. Susceptibility measurements [Fig. 10(b)] show a magnetic transition around $T_F \approx 72$ K, which has been attributed to a magnetic interaction with frustration in the kagome lattice.[38] Heavy fermion behavior was also captured by the heat capacity measurement in $CsCr_6Sb_6$.[38] A prominent flat band at the Fermi level, spanning the entire Brillouin zone, was observed through ARPES measurement [Figs. 10(c)–10(e)].[38] This flat band is believed to arise from the destructive interference of Cr-3d orbitals in the kagome geometry with strong electron correlation [Figs. 10(f)–10(g)]. Thanks to the van der Waals nature, $CsCr_6Sb_6$ shows a strong dimensional tunability of Kondo physics and serves as an excellent platform for studying Kondo physics and related quantum criticality in frustrated lattices, without the involvement of localized f-orbitals.[38] Furthermore, in another kagome metal, Ni_3In,[36] Kondo-induced heavy fermion behavior was also reported.

6.2. Topological flat band

In heavy fermion systems, strongly localized f-orbitals contribute to dispersionless flat bands in momentum space, accompanied by strong electron correlations. These flat bands, however, do not exhibit any topological characteristics. In contrast, kagome lattices give rise to flat bands that result from destructive interference and can exhibit non-trivial topology, known as topological flat bands. Similar to Dirac points, spin–orbit coupling (SOC) plays a crucial role in these topological flat bands, opening a gap between the dispersionless and dispersive branches [Fig. 11(a)]. In the absence of magnetism, SOC induces a spin Chern gap, with divergent spin Berry curvature [Fig. 11(a)]. Out-of-plane ferromagnetism can further enhance this gap, transforming it into a Chern gap. The partial filling of such topological flat bands can facilitate the emergence of fractional topological excitations.[6,83]

While transport measurements can provide insight into the topological properties of materials, they are generally limited to states near the Fermi level. In contrast, ARPES can directly probe all occupied states below the Fermi level. Moreover, utilizing circular dichroism (CD), ARPES, and spin-resolved ARPES can allow for the direct characterization of the Berry curvature and spin Berry curvature of quantum materials, providing a powerful tool to unravel the non-trivial quantum geometry of these systems.[71,84]

In kagome materials, flat bands arise from the unique destructive interference mechanism inherent in their lattice geometry. However, in real materials, strong interlayer coupling and hybridization between kagome orbitals and other atomic orbitals can disrupt the formation of these dispersionless bands. As a result, real systems exhibiting both flat bands and non-trivial topologies induced by strong SOC are rare. In the kagome metal CoSn, two topologically protected flat bands originating from Co-3d orbitals were identified near the Fermi level through synchrotron-based ARPES.[15,85] One of these bands, dominated by in-plane orbitals, lies at the Fermi level, while the other, dominated by out-of-plane orbitals, is located approximately 0.27 eV below the Fermi level [Figs. 11(b) and 11(c)]. Spin–orbit coupling opens a substantial gap of 80 meV between the flat and dispersive bands. Since CoSn is a non-magnetic metal, this flat band is classified as exhibiting a Z_2 topology.[15] Anisotropic resistivity and magnetic susceptibility measurements in CoSn suggest orbital magnetism arising from the non-trivial Berry curvature associated with the topological flat band at the Fermi level.[86]

In addition to CoSn, another Ti-based kagome material, ATi_3Bi_5 (A = K, Rb, Cs), has been shown to host topological flat bands.[87] ATi_3Bi_5 shares a similar crystal structure with the well-known kagome compound AV_3Sb_5, but the replacement of V atoms by Ti atoms shifts the chemical potential from the van Hove singularities (vHSs) to a position closer to the flat band.[88] While no charge density wave (CDW) has been observed in ATi_3Bi_5, spectroscopic studies have suggested the presence of electronic nematic orders,[87,89] potentially driven by strong inter-orbital coupling.[90] This rotation-symmetry-breaking order may share origins with the electron nematicity found in AV_3Sb_5.[33] Additionally, ARPES has revealed a topological flat band at approximately 0.25 eV below the Fermi level [Figs. 11(d) and 11(e)], coexisting with multiple non-trivial Dirac fermions.[88,91]

In another class of kagome materials, the '166' type RV_6Sn_6 (R = Tb, Ho, Sc), topological flat bands have been observed through CD-ARPES.[92] By using circularly polarized light, the local orbital magnetic moment induced by the Berry curvature of the flat band can be detected. As shown in Fig. 11(f), a dispersionless electronic state arising from the kagome lattice is located about 1 eV below the Fermi level. Spin-resolved CD-ARPES [Figs. 11(g)–11(i)] further confirms the presence of spin Berry curvature associated with the topological flat band, consistent with first-principles predictions.[92]

6.3. Three-dimensional flat band in pyrochlore lattice

The rich nature in the kagome lattice is predominantly confined to the two-dimensional systems. In contrast, the

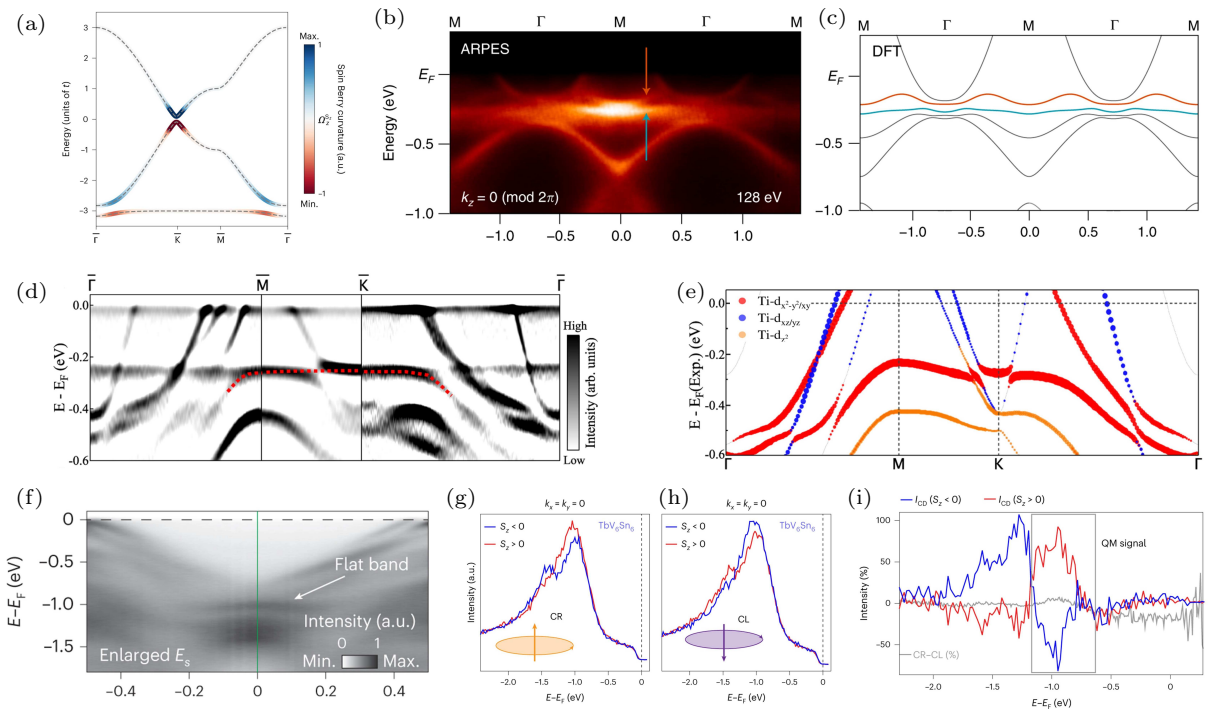


Fig. 11. Observation of topological flat band in kagome materials CoSn, ATi_3Bi_5 and RV_6Sn_6. (a) Tight-binding band structures of kagome lattice with SOC. The spin Berry curvature is represented by the color. (b) Observation of SOC-induced topological flat band (marked by arrows) in CoSn. (c) DFT calculated band structure along the same direction with (b) when considering SOC. The topological flat bands are marked by the colored lines. (d) Observation of SOC-induced topological flat band (marked by the red dashed line) in $CsTi_3Bi_5$. (e) DFT calculated band structure along the same direction of (d) considering SOC. (f) Observation of SOC-induced topological flat band in TbV_6Sn_6. (g) Circular right (CR) spin-ARPES energy distribution curves (EDC) extracted from the BZ center to prevent geometrical dichroism effect. (h) Same as (g) but under the circular left (CL) polarization. (i) Spin-resolved circular dichroism intensity from (g) and (h). Panel (a) adapted from Ref. [15]. Panels (b) and (c) adapted from Ref. [15]. Panels (d) and (e) adapted from Ref. [88]. Panels (f)–(i) adapted from Ref. [92].

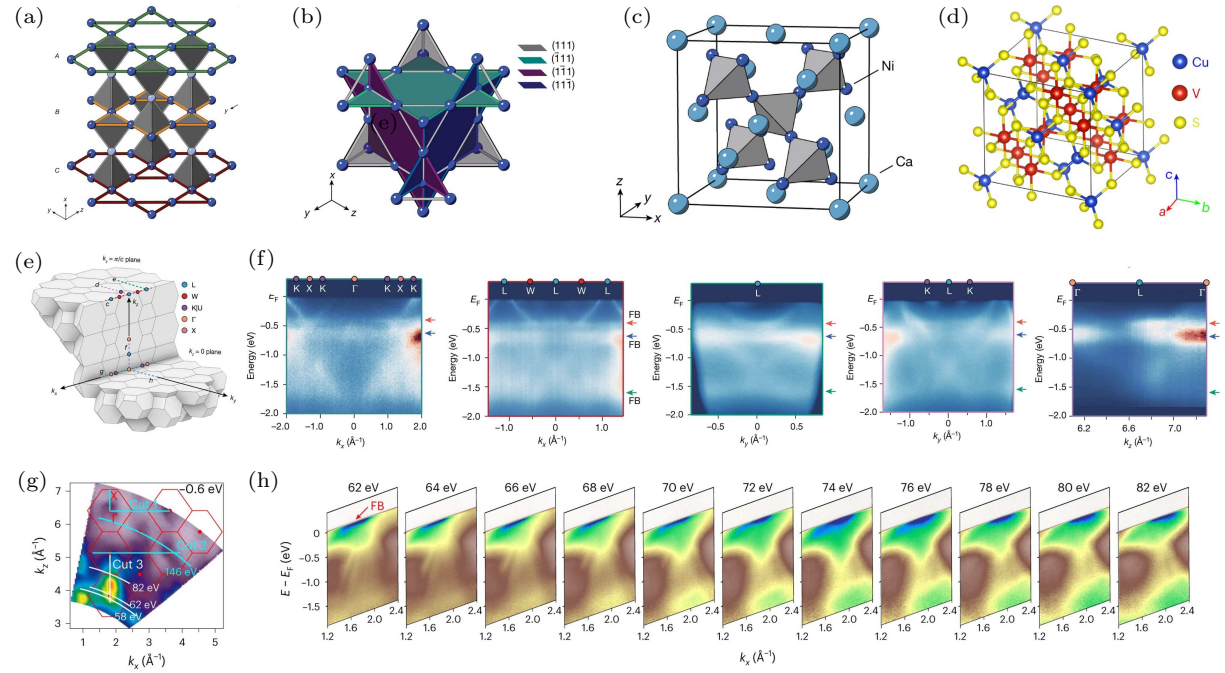


Fig. 12. Three-dimensional flat band in pyrochlore metal $CaNi_2$ and CuV_2S_4. (a) Schematic illustration showing the pyrochlore lattice consists of ABC stacking kagome lattice along the 111 direction as illustrated in panel (b). (c) Crystal structure of $CaNi_2$ with the pyrochlore lattice formed by Ni atoms. (d) Crystal structure of CuV_2S_4 with the pyrochlore lattice formed by V atoms. (e) Schematic illustration of three-dimensional Brillouin zones of $CaNi_2$. Colored dashed lines mark the momentum directions of the ARPES data in panel (f). (f) Measured band structures along the high symmetry direction of $CaNi_2$. The flat bands expand across the whole three-dimensional Brillouin zone as marked by the arrows. (g) ARPES mapping at -0.6 eV measured for different photon energies with respect to the (001) surface of CuV_2S_4. (h) Observation of flat band expanding over the whole three-dimensional Brillouin zone at the Fermi level of CuV_2S_4. Panels (a)–(c) adapted from Ref. [97]. Panel (d) adapted from Ref. [37]. Panels (e) and (f) adapted from Ref. [97]. Panels (g) and (h) adapted from Ref. [37].

pyrochlore lattice — a three-dimensional frustrated network composed of corner-sharing tetrahedra — provides a natural extension of these unique electronic states into three-dimensional materials [Figs. 12(a)–12(h)]. This lattice can be conceptualized as a stack of 2D kagome lattices aligned along the four diagonal directions [Figs. 12(a) and 12(b)]. Like kagome materials, pyrochlore materials are also poised to realize a range of novel physical phenomena, generating significant interest in the scientific community.[93–96]

Recent ARPES studies on several pyrochlore materials have identified kagome-like electronic states extending throughout three-dimensional momentum space. For example, in $CaNi_2$ [Fig. 12(c)], ARPES data obtained at varying photon energies revealed multiple flat bands across the entire 3D Brillouin zone [Figs. 12(e) and 12(f)]. By chemically doping the material to align these flat bands with the Fermi level, electron correlation is enhanced, triggering superconductivity.[97] This finding has spurred further exploration of pyrochlore materials with similar electronic characteristics. In the case of CuV_2S_4 [Fig. 12(d)], ARPES measurements also captured three-dimensional flat bands near the Fermi level, alongside non-Fermi-liquid behavior and emerging charge order [Figs. 12(g) and 12(h)].[37] Similarly, in the pyrochlore superconductor $CeRu_2$, 3D flat bands and Dirac cones were observed.[98] Collectively, these results offer a promising avenue to extend kagome-inspired physics into higher-dimensional systems.

7. Outlook

In recent years, the growing interest in kagome materials has highlighted their pivotal role in the realm of quantum materials, acting as a bridge between the study of correlated physics and topological phases. Several comprehensive reviews have already summarized the current state and future prospects of kagome quantum materials.[1,2] In this paper, we focus on the future research directions of kagome materials, with a particular emphasis on the application of ARPES in advancing our understanding of these systems.

Despite significant progress, the exploration of kagome materials is still in its early stages, with many potential kagome compounds and their applications yet to be uncovered. This underscores the need for further efforts in material synthesis to discover new candidates. Concurrently, detailed spectroscopic investigations are crucial to unravel the complex and rich physics of the intriguing kagome materials that have already been identified. For instance, the classical kagome superconducting family RT_3X_2 (R = rare earth, T = transition metal, X = Si, Ga, B) exhibits superconductivity with unconventional characteristics in the strong correlation regime, warranting deeper spectroscopic studies.[99–102] Additionally, the recently discovered 134-type distorted kagome magnets have garnered significant attention due to their intriguing properties.[103–105]

Moreover, many of the kagome materials discovered to date exhibit remarkable tunability of their exotic quantum states. This tunability can be achieved using conventional methods such as chemical doping or electrostatic gating to adjust the Fermi level, as well as by applying strain, magnetic fields, or altering dimensionality. These approaches allow for the manipulation of various quantum phases, facilitating the exploration of novel physics and potential device applications. When combined with ARPES, these tuning techniques enable real-time, *in-situ* observations of the evolution of electronic states under external perturbations.[106–108] This integrated approach provides a powerful framework for investigating the rich many-body physics inherent in kagome materials.

Recently, with advancements in ultrafast laser technology, time-resolved ARPES has become a powerful tool in the study of quantum materials.[109] Time-resolved ARPES enables the investigation of complex dynamics in kagome materials on ultrafast timescales, providing insights into their temporal evolution.[110] The introduction of strong-field lasers further opens up new avenues for controlling a variety of quantum states within these systems.

The realization of kagome-like electronic structures in artificial systems has emerged as a key research frontier. Artificial materials, engineered through molecular design and nanotechnology, present a promising platform for realizing nontrivial quantum states akin to those found in kagome lattices.[111–113] Similarly, moiré engineering, which manipulates the alignment of two-dimensional materials to generate moiré patterns, offers exciting possibilities for the emergence of kagome-like electronic behaviors.[114,115] At present, tunneling spectroscopy techniques[111–113] are predominantly used to probe these artificial kagome states. However, with the development of nano-ARPES,[11] future advancements will enable direct momentum-space observations of these artificial kagome electronic states.

Acknowledgments

Project supported by the National Natural Science Foundation of China (Grant Nos. 12488201, 12074411, 12374066, 12374154, and 12494593), the National Key Research and Development Program of China (Grant No. 2022YFA1403900, 2021YFA1401800, 2022YFA1604200, 2023YFA1406002, 2024YFA1408301, and 2024YFA1400026), the Strategic Priority Research Program (B) of the Chinese Academy of Sciences (Grant Nos. XDB25000000 and XDB33000000), the Innovation Program for Quantum Science and Technology (Grant No. 2021ZD0301800), the Youth Innovation Promotion Association of CAS (Grant No. Y2021006), and Synergetic Extreme Condition User Facility (SECUF).

References

[1] Yin J X, Lian B and Hasan M Z 2022 *Nature* **612** 647
[2] Wang Y, Wu H, McCandless G T, Chan J Y and Ali M N 2023 *Nat. Rev. Phys.* **5** 635
[3] Sachdev S 1992 *Phys. Rev. B* **45** 12377
[4] Balents L 2010 *Nature* **464** 199
[5] Guo H M and Franz M 2009 *Phys. Rev. B* **80** 113102
[6] Tang E, Mei J W and Wen X G 2011 *Phys. Rev. Lett.* **106** 236802
[7] Kiesel M L and Thomale R 2012 *Phys. Rev. B* **86** 121105
[8] Kiesel M L, Platt C and Thomale R 2013 *Phys. Rev. Lett.* **110** 126405
[9] Mazin I I, Jeschke H O, Lechermann F, Lee H, Fink M, Thomale R and Valentí R 2014 *Nat. Commun.* **5** 4261
[10] Sobota J A, He Y and Shen Z X 2021 *Rev. Mod. Phys.* **93** 025006
[11] Zhang H, Pincelli T, Jozwiak C, Kondo T, Ernstorfer R, Sato T and Zhou S 2022 *Nature Reviews Methods Primers* **2** 54
[12] Mielke A 1991 *J. Phys. A: Math. Gen.* **24** L73
[13] Mielke A 1991 *J. Phys. A: Math. Gen.* **24** 3311
[14] Mielke A 1992 *J. Phys. A: Math. Gen.* **25** 4335
[15] Kang M, Fang S, Ye L, Po H C, Denlinger J, Jozwiak C, Bostwick A, Rotenberg E, Kaxiras E, Checkelsky J G and Comin R 2020 *Nat. Commun.* **11** 4004
[16] Ye L D, Kang M G, Liu J W, von Cube F, Wicker C R, Suzuki T, Jozwiak C, Bostwick A, Rotenberg E, Bell D C, Fu L, Comin R and Checkelsky J G 2018 *Nature* **555** 638
[17] Ohgushi K, Murakami S and Nagaosa N 2000 *Phys. Rev. B* **62** R6065
[18] Zhang Z Y 2011 *J. Phys. Condens. Matter* **23** 365801
[19] Xu G, Lian B and Zhang S C 2015 *Phys. Rev. Lett.* **115** 186802
[20] Yang S, Gu Z C, Sun K and Das Sarma S 2012 *Phys. Rev. B* **86** 241112
[21] Burkov A A and Balents L 2011 *Phys. Rev. Lett.* **107** 127205
[22] Liu E K, Sun Y, Kumar N, Muechler L, Sun A L, Jiao L, Yang S Y, Liu D F, Liang A J, Xu Q N, Kroder J, Süss V, Borrmann H, Shekhar C, Wang Z S, Xi C Y, Wang W H, Schnelle W, Wirth S, Chen Y L, Goennenwein S T B and Felser C 2018 *Nat. Phys.* **14** 1125
[23] Nakatsuji S, Kiyohara N and Higo T 2015 *Nature* **527** 212
[24] Kuroda K, Tomita T, Suzuki M T, Bareille C, Nugroho A, Goswami P, Ochi M, Ikhlas M, Nakayama M, Akebi S, Noguchi R, Ishii R, Inami N, Ono K, Kumigashira H, Varykhalov A, Muro T, Koretsune T, Arita R, Shin S, Kondo T and Nakatsuji S 2017 *Nat. Mater.* **16** 1090
[25] Wang W S, Li Z Z, Xiang Y Y and Wang Q H 2013 *Phys. Rev. B* **87** 115135
[26] Yu S L and Li J X 2012 *Phys. Rev. B* **85** 144402
[27] Ge J, Wang P, Xing Y, Yin Q, Wang A, Shen J, Lei H, Wang Z and Wang J 2024 *Phys. Rev. X* **14** 021025
[28] Le T, Pan Z, Xu Z, Liu J, Wang J, Lou Z, Yang X, Wang Z, Yao Y, Wu C and Lin X 2024 *Nature* **630** 64
[29] Li H, Zhang T T, Yilmaz T, Pai Y Y, Marvinney C E, Said A, Yin Q W, Gong C S, Tu Z J, Vescovo E, Nelson C S, Moore R G, Murakami S, Lei H C, Lee H N, Lawrie B J and Miao H 2021 *Phys. Rev. X* **11** 031050
[30] Jiang Y X, Yin J X, Denner M M, Shumiya N, Ortiz B R, Xu G, Guguchia Z, He J, Hossain M S, Liu X, Ruff J, Kautzsch L, Zhang S S, Chang G, Belopolski I, Zhang Q, Cochran T A, Multer D, Litskevich M, Cheng Z J, Yang X P, Wang Z, Thomale R, Neupert T, Wilson S D and Hasan M Z 2021 *Nat. Mater.* **20** 1353
[31] Mielke C, Das D, Yin J X, Liu H, Gupta R, Jiang Y X, Medarde M, Wu X, Lei H C, Chang J, Dai P C, Si Q, Miao H, Thomale R, Neupert T, Shi Y, Khasanov R, Hasan M Z, Luetkens H and Guguchia Z 2022 *Nature* **602** 245
[32] Chen H, Yang H T, Hu B, Zhao Z, Yuan J, Xing Y Q, Qian G J, Huang Z H, Li G, Ye Y H, Ma S, Ni S L, Zhang H, Yin Q W, Gong C S, Tu Z J, Lei H C, Tan H X, Zhou S, Shen C M, Dong X L, Yan B H, Wang Z Q and Gao H J 2021 *Nature* **599** 222
[33] Nie L P, Sun K, Ma W R, Song D W, Zheng L X, Liang Z W, Wu P, Yu F H, Li J, Shan M, Zhao D, Li S J, Kang B L, Wu Z M, Zhou Y B, Liu K, Xiang Z J, Ying J J, Wang Z Y, Wu T and Chen X H 2022 *Nature* **604** 59
[34] Zhou S and Wang Z 2022 *Nat. Commun.* **13** 7288
[35] Gao S, Zhang S, Wang C, Yan S, Han X, Ji X, Tao W, Liu J, Wang T, Yuan S, Qu G, Chen Z, Zhang Y, Huang J, Pan M, Peng S, Hu Y, Li H, Huang Y, Zhou H, Meng S, Yang L, Wang Z, Yao Y, Chen Z, Shi M, Ding H, Yang H, Jiang K, Li Y, Lei H, Shi Y, Weng H and Qian T 2023 *Phys. Rev. X* **13** 041049
[36] Ye L, Fang S, Kang M, Kaufmann J, Lee Y, John C, Neves P M, Zhao S Y F, Denlinger J, Jozwiak C, Bostwick A, Rotenberg E, Kaxiras E, Bell D C, Janson O, Comin R and Checkelsky J G 2024 *Nat. Phys.* **20** 610
[37] Huang J, Chen L, Huang Y, Setty C, Gao B, Shi Y, Liu Z, Zhang Y, Yilmaz T, Vescovo E, Hashimoto M, Lu D, Yakobson B I, Dai P, Chu J H, Si Q and Yi M 2024 *Nat. Phys.* **20** 603
[38] Song B, Xie Y, Li W J, Liu H, Zhang Q, Guo J g, Zhao L, Yu S L, Zhou X, Chen X and Ying T arXiv:2404.12374 [cond-mat.str-el]
[39] Checkelsky J G, Bernevig B A, Coleman P, Si Q and Paschen S 2024 *Nature Reviews Materials* **9** 509
[40] Jovanovic M and Schoop L M 2022 *J. Am. Chem. Soc.* **144** 10978
[41] Damascelli A, Hussain Z and Shen Z X 2003 *Rev. Mod. Phys.* **75** 473
[42] Ortiz B R, Gomes L C, Morey J R, Winiarski M, Bordelon M, Mangum J S, Oswald I W H, Rodriguez-Rivera J A, Neilson J R, Wilson S D, Ertekin E, McQueen T M and Toberer E S 2019 *Phys. Rev. Mater.* **3** 094407
[43] Ortiz B R, Teicher S M L, Hu Y, Zuo J L, Sarte P M, Schueller E C, Abeykoon A M M, Krogstad M J, Rosenkranz S, Osborn R, Seshadri R, Balents L, He J and Wilson S D 2020 *Phys. Rev. Lett.* **125** 247002
[44] Yang S Y, Wang Y, Ortiz B R, Liu D, Gayles J, Derunova E, Gonzalez-Hernandez R, Šmejkal L, Chen Y, Parkin S S P, Wilson S D, Toberer E S, McQueen T and Ali M N 2020 *Sci. Adv.* **6** eabb6003
[45] Luo H, Gao Q, Liu H, Gu Y, Wu D, Yi C, Jia J, Wu S, Luo X, Xu Y, Zhao L, Wang Q, Mao H, Liu G, Zhu Z, Shi Y, Jiang K, Hu J, Xu Z and Zhou X J 2022 *Nat. Commun.* **13** 273
[46] Hu Y, Wu X, Ortiz B R, Ju S, Han X, Ma J, Plumb N C, Radovic M, Thomale R, Wilson S D, Schnyder A P and Shi M 2022 *Nat. Commun.* **13** 2220
[47] Liang Z, Hou X, Zhang F, Ma W, Wu P, Zhang Z, Yu F, Ying J J, Jiang K, Shan L, Wang Z and Chen X H 2021 *Phys. Rev. X* **11** 031026
[48] Feng X, Jiang K, Wang Z and Hu J 2021 *Science Bulletin* **66** 1384
[49] Denner M M, Thomale R and Neupert T 2021 *Phys. Rev. Lett.* **127** 217601
[50] Simon M E and Varma C M 2002 *Phys. Rev. Lett.* **89** 247003
[51] Haldane F D M 1988 *Phys. Rev. Lett.* **61** 2015
[52] Kang M, Fang S, Kim J K, Ortiz B R, Ryu S H, Kim J, Yoo J, Sangiovanni G, Di Sante D, Park B G, Jozwiak C, Bostwick A, Rotenberg E, Kaxiras E, Wilson S D, Park J H and Comin R 2022 *Nat. Phys.* **18** 301
[53] Liu Z, Zhao N, Yin Q, Gong C, Tu Z, Li M, Song W, Liu Z, Shen D, Huang Y, Liu K, Lei H and Wang S 2021 *Phys. Rev. X* **11** 041010
[54] Zhong Y G, Li S Z, Liu H X, Dong Y Y, Aido K, Arai Y, Li H X, Zhang W L, Shi Y G, Wang Z Q, Shin S, Lee H N, Miao H, Kondo T and Okazaki K 2023 *Nat. Commun.* **14** 1945
[55] Zhong Y G, Liu J J, Wu X X, Guguchia Z, Yin J X, Mine A, Li Y K, Najafzadeh S, Das D, Mielke C, Khasanov R, Luetkens H, Suzuki T, Liu K C, Han X L, Kondo T, Hu J P, Shin S, Wang Z W, Shi X, Yao Y G and Okazaki K 2023 *Nature* **617** 488
[56] Teng X K, Chen L B, Ye F, Rosenberg E, Liu Z Y, Yin J X, Jiang Y X, Oh J S, Hasan M Z, Neubauer K J, Gao B, Xie Y F, Hashimoto M, Lu D H, Jozwiak C, Bostwick A, Rotenberg E, Birgeneau R J, Chu J H, Yi M and Dai P C 2022 *Nature* **609** 490
[57] Ohoyama T, Yasukochi K and Kanematsu K 1963 *J. Phys. Soc. Jpn.* **18** 589
[58] Beckman O, Carrander K, Lundgren L and Richardson M 1972 *Phys. Scr.* **6** 151
[59] Yin J X, Jiang Y X, Teng X K, Hossain M S, Mardanya S, Chang T R, Ye Z J, Xu G, Denner M M, Neupert T, Lienhard B, Deng H B, Setty C, Si Q M, Chang G Q, Guguchia Z, Gao B, Shumiya N, Zhang Q, Cochran T A, Muller D, Yi M, Dai P C and Hasan M Z 2022 *Phys. Rev. Lett.* **129** 166401
[60] Teng X K, Oh J S, Tan H X, Chen L B, Huang J W, Gao B, Yin J X, Chu J H, Hashimoto M, Lu D H, Jozwiak C, Bostwick A, Rotenberg E, Granroth G E, Yan B H, Birgeneau R J, Dai P C and Yi M 2023 *Nat. Phys.* **19** 814
[61] Wu L, Hu Y, Fan D, Wang D and Wan X 2023 *Chin. Phys. Lett.* **40** 117103
[62] Kida T, Fenner L A, Dee A A, Terasaki I, Hagiwara M and Wills A S 2011 *J. Phys.: Condens. Matter* **23** 112205
[63] Ekahana S A, Soh Y, Tamai A, Gosálbez-Martínez D, Yao M, Hunter A, Fan W, Wang Y, Li J, Kleibert A, Vaz C A F, Ma J, Lee H, Xiong Y, Yazyev O V, Baumberger F, Shi M and Aeppli G 2024 *Nature* **627** 67

[64] Yin J X, Zhang S S, Li H, Jiang K, Chang G, Zhang B, Lian B, Xiang C, Belopolski I, Zheng H, Cochran T A, Xu S Y, Bian G, Liu K, Chang T R, Lin H, Lu Z Y, Wang Z, Jia S, Wang W and Hasan M Z 2018 *Nature* **562** 91

[65] Yin J X, Ma W, Cochran T A, Xu X, Zhang S S, Tien H J, Shumiya N, Cheng G, Jiang K, Lian B, Song Z, Chang G, Belopolski I, Multer D, Litskevich M, Cheng Z J, Yang X P, Swidler B, Zhou H, Lin H, Neupert T, Wang Z, Yao N, Chang T R, Jia S and Zahid Hasan M 2020 *Nature* **583** 533

[66] Li M, Wang Q, Wang G, Yuan Z, Song W, Lou R, Liu Z, Huang Y, Liu Z, Lei H, Yin Z and Wang S 2021 *Nat. Commun.* **12** 3129

[67] Xu Q, Liu E, Shi W, Muechler L, Gayles J, Felser C and Sun Y 2018 *Phys. Rev. B* **97** 235416

[68] Liu D F, Liang A J, Liu E K, Xu Q N, Li Y W, Chen C, Pei D, Shi W J, Mo S K, Dudin P, Kim T, Cacho C, Li G, Sun Y, Yang L X, Liu Z K, Parkin S S P, Felser C and Chen Y L 2019 *Science* **365** 1282

[69] Belopolski I, Cochran T A, Liu X, Cheng Z J, Yang X P, Guguchia Z, Tsirkin S S, Yin J X, Vir P, Thakur G S, Zhang S S, Zhang J, Kaznatcheev K, Cheng G, Chang G, Multer D, Shumiya N, Litskevich M, Vescovo E, Kim T K, Cacho C, Yao N, Felser C, Neupert T and Hasan M Z 2021 *Phys. Rev. Lett.* **127** 256403

[70] Liu D F, Xu Q N, Liu E K, Shen J L, Le C C, Li Y W, Pei D, Liang A J, Dudin P, Kim T K, Cacho C, Xu Y F, Sun Y, Yang L X, Liu Z K, Felser C, Parkin S S P and Chen Y L 2021 *Phys. Rev. B* **104** 205140

[71] Kang M, Kim S, Qian Y, Neves P M, Ye L, Jung J, Puntel D, Mazzola F, Fang S, Jozwiak C, Bostwick A, Rotenberg E, Fuji J, Vobornik I, Park J H, Checkelsky J G, Yang B J and Comin R 2025 *Nat. Phys.* **21** 110

[72] Zaanen J, Sawatzky G A and Allen J W 1985 *Phys. Rev. Lett.* **55** 418

[73] Hu C, Zhao J, Gao Q, Yan H, Rong H, Huang J, Liu J, Cai Y, Li C, Chen H, Zhao L, Liu G, Jin C, Xu Z, Xiang T and Zhou X J 2021 *Nat. Commun.* **12** 1356

[74] Sun Z, Zhou H, Wang C, Kumar S, Geng D, Yue S, Han X, Haraguchi Y, Shimada K, Cheng P, Chen L, Shi Y, Wu K, Meng S and Feng B 2022 *Nano Lett.* **22** 4596

[75] Regmi S, Fernando T, Zhao Y, Sakhya A P, Dhakal G, Bin Elius I, Vazquez H, Denlinger J D, Yang J, Chu J H, Xu X, Cao T and Neupane M 2022 *Communications Materials* **3** 100

[76] Grytsiuk S, Katsnelson M I, Loon E G C P V and Rösner M 2024 *npj Quantum Materials* **9** 8

[77] Hu J, Zhang X, Hu C, Sun J, Wang X, Lin H Q and Li G 2023 *Communications Physics* **6** 172

[78] Haraguchi Y, Michioka C, Ishikawa M, Nakano Y, Yamochi H, Ueda H and Yoshimura K 2017 *Inorganic Chemistry* **56** 3483

[79] Pasco C M, El Baggari I, Bianco E, Kourkoutis L F and McQueen T M 2019 *ACS Nano* **13** 9457

[80] Zhang Y, Gu Y, Weng H, Jiang K and Hu J 2023 *Phys. Rev. B* **107** 035126

[81] Regmi S, Sakhya A P, Fernando T, Zhao Y, Jeff D, Sprague M, Gonzalez F, Bin Elius I, Mondal M I, Valadez N, Jarrett D, Agosto A, Yang J, Chu J H, Khondaker S I, Xu X, Cao T and Neupane M 2023 *Phys. Rev. B* **108** L121404

[82] Yang Y f, Fisk Z, Lee H O, Thompson J D and Pines D 2008 *Nature* **454** 611

[83] Okamoto S, Mohanta N, Dagotto E and Sheng D N 2022 *Communications Physics* **5** 198

[84] Schüler M, De Giovannini U, Hübener H, Rubio A, Sentef M A and Werner P 2020 *Sci. Adv.* **6** eaay2730

[85] Liu Z, Li M, Wang Q, Wang G, Wen C, Jiang K, Lu X, Yan S, Huang Y, Shen D, Yin J X, Wang Z, Yin Z, Lei H and Wang S 2020 *Nat. Commun.* **11** 4002

[86] Huang H, Zheng L, Lin Z, Guo X, Wang S, Zhang S, Zhang C, Sun Z, Wang Z, Weng H, Li L, Wu T, Chen X and Zeng C 2022 *Phys. Rev. Lett.* **128** 096601

[87] Yang H, Ye Y, Zhao Z, Liu J, Yi X W, Zhang Y, Xiao H, Shi J, You J Y, Huang Z, Wang B, Wang J, Guo H, Lin X, Shen C, Zhou W, Chen H, Dong X, Su G, Wang Z and Gao H J 2024 *Nat. Commun.* **15** 9626

[88] Yang J, Yi X, Zhao Z, Xie Y, Miao T, Luo H, Chen H, Liang B, Zhu W, Ye Y, You J Y, Gu B, Zhang S, Zhang F, Yang F, Wang Z, Peng Q, Mao H, Liu G, Xu Z, Chen H, Yang H, Su G, Gao H, Zhao L and Zhou X J 2023 *Nat. Commun.* **14** 4089

[89] Li H, Cheng S, Ortiz B R, Tan H, Werhahn D, Zeng K, Johrendt D, Yan B, Wang Z, Wilson S D and Zeljkovic I 2023 *Nat. Phys.* **19** 1591

[90] Hu Y, Le C, Zhang Y, Zhao Z, Liu J, Ma J, Plumb N C, Radovic M, Chen H, Schnyder A P, Wu X, Dong X, Hu J, Yang H, Gao H J and Shi M 2023 *Nat. Phys.* **19** 1827

[91] Jiang Z, Liu Z, Ma H, Xia W, Liu Z, Liu J, Cho S, Yang Y, Ding J, Liu J, Huang Z, Qiao Y, Shen J, Jing W, Liu X, Liu J, Guo Y and Shen D 2023 *Nat. Commun.* **14** 4892

[92] Di Sante D, Bigi C, Eck P, Enzner S, Consiglio A, Pokharel G, Carrara P, Orgiani P, Polewczyk V, Fujii J, King P D C, Vobornik I, Rossi G, Zeljkovic I, Wilson S D, Thomale R, Sangiovanni G, Panaccione G and Mazzola F 2023 *Nat. Phys.* **19** 1135

[93] Guo H M and Franz M 2009 *Phys. Rev. Lett.* **103** 206805

[94] Pesin D and Balents L 2010 *Nat. Phys.* **6** 376

[95] Tian Z, Kohama Y, Tomita T, Ishizuka H, Hsieh T H, Ishikawa J J, Kindo K, Balents L and Nakatsuji S 2016 *Nat. Phys.* **12** 134

[96] Jiang W, de Sousa D J P, Wang J P and Low T 2021 *Phys. Rev. Lett.* **126** 106601

[97] Wakefield J P, Kang M, Neves P M, Oh D, Fang S, McTigue R, Frank Zhao S Y, Lamichhane T N, Chen A, Lee S, Park S, Park J H, Jozwiak C, Bostwick A, Rotenberg E, Rajapitamahuni A, Vescovo E, McChesney J L, Graf D, Palmstrom J C, Suzuki T, Li M, Comin R and Checkelsky J G 2023 *Nature* **623** 301

[98] Huang J, Setty C, Deng L, You J Y, Liu H, Shao S, Oh J S, Guo Y, Zhang Y, Yue Z, Yin J X, Hashimoto M, Lu D, Gorovikov S, Dai P, Denlinger J D, Allen J W, Hasan M Z, Feng Y P, Birgeneau R J, Shi Y, Chu C W, Chang G, Si Q and Yi M 2024 *npj Quantum Materials* **9** 71

[99] Plokhikh I, Mielke C, Nakamura H, Petricek V, Qin Y, Sazgari V, Küspert J, Biało I, Shin S, Ivashko O, Graham J N, Zimmermann M V, Medarde M, Amato A, Khasanov R, Luetkens H, Fischer M H, Hasan M Z, Yin J X, Neupert T, Chang J, Xu G, Nakatsuji S, Pomjakushina E, Gawryluk D J and Guguchia Z 2024 *Communications Physics* **7** 182

[100] Gui X and Cava R J 2022 *Chemistry of Materials* **34** 2824

[101] Chakrabortty S, Kumar R and Mohapatra N 2023 *Phys. Rev. B* **107** 024503

[102] Chaudhary S, Shama, Singh J, Consiglio A, Di Sante D, Thomale R and Singh Y 2023 *Phys. Rev. B* **107** 085103

[103] Ortiz B R, Pokharel G, Gundayao M, Li H, Kaboudvand F, Kautzsch L, Sarker S, Ruff J P C, Hogan T, Alvarado S J G, Sarte P M, Wu G, Braden T, Seshadri R, Toberer E S, Zeljkovic I and Wilson S D 2023 *Phys. Rev. Mater.* **7** 064201

[104] Ortiz B R, Miao H, Parker D S, Yang F, Samolyuk G D, Clements E M, Rajapitamahuni A, Yilmaz T, Vescovo E, Yan J, May A F and McGuire M A 2023 *Chemistry of Materials* **35** 9756

[105] Chen L, Zhou Y, Zhang H, Ji X, Liao K, Ji Y, Li Y, Guo Z, Shen X, Yu R, Yu X, Weng H and Wang G 2024 *Communications Materials* **5** 73

[106] Hossain M A, Mottershead J D F, Fournier D, Bostwick A, McChesney J L, Rotenberg E, Liang R, Hardy W N, Sawatzky G A, Elfimov I S, Bonn D A and Damascelli A 2008 *Nat. Phys.* **4** 527

[107] Riccò S, Kim M, Tamai A, McKeown Walker S, Bruno F Y, Cucchi I, Cappelli E, Besnard C, Kim T K, Dudin P, Hoesch M, Gutmann M J, Georges A, Perry R S and Baumberger F 2018 *Nat. Commun.* **9** 4535

[108] Huang J, Yue Z, Baydin A, Zhu H, Nojiri H, Kono J, He Y and Yi M 2023 *Rev. Sci. Instrum.* **94** 093902

[109] Boschini F, Zonno M and Damascelli A 2024 *Rev. Mod. Phys.* **96** 015003

[110] Azoury D, von Hoegen A, Su Y, Oh K H, Holder T, Tan H, Ortiz B R, Capa Salinas A, Wilson S D, Yan B and Gedik N 2023 *Proc. Natl. Acad. Sci. USA* **120** e2308588120

[111] Kempkes S N, Slot M R, van den Broeke J J, Capiod P, Benalcazar W A, Vanmaekelbergh D, Bercioux D, Swart I and Morais Smith C 2019 *Nat. Mater.* **18** 1292

[112] Huang L, Kong X, Zheng Q, Xing Y, Chen H, Li Y, Hu Z, Zhu S, Qiao J, Zhang Y Y, Cheng H, Cheng Z, Qiu X, Liu E, Lei H, Lin X, Wang Z, Yang H, Ji W and Gao H J 2023 *Nat. Commun.* **14** 5230

[113] Yin R, Zhu X, Fu Q, Hu T, Wan L, Wu Y, Liang Y, Wang Z, Qiu Z L, Tan Y Z, Ma C, Tan S, Hu W, Li B, Wang Z F, Yang J and Wang B 2024 *Nat. Commun.* **15** 2969

[114] Li Z, Zhuang J, Wang L, Feng H, Gao Q, Xu X, Hao W, Wang X, Zhang C, Wu K, Dou S X, Chen L, Hu Z and Du Y 2018 *Sci. Adv.* **4** eaau4511

[115] Crasto de Lima F, Miwa R H and Suárez Morell E 2019 *Phys. Rev. B* **100** 155421

[116] Kang M, Ye L, Fang S, You J S, Levitan A, Han M, Facio J I, Jozwiak C, Bostwick A, Rotenberg E, Chan M K, McDonald R D, Graf D, Kaznatcheev K, Vescovo E, Bell D C, Kaxiras E, van den Brink J, Richter M, Prasad Ghimire M, Checkelsky J G and Comin R 2020 *Nat. Mater.* **19** 163

[117] Sales B C, Yan J, Meier W R, Christianson A D, Okamoto S and McGuire M A 2019 *Phys. Rev. Mater.* **3** 114203

[118] Ren Z, Huang J, Tan H, Biswas A, Pulkkinen A, Zhang Y, Xie Y, Yue Z, Chen L, Xie F, Allen K, Wu H, Ren Q, Rajapitamahuni A, Kundu A K, Vescovo E, Kono J, Morosan E, Dai P, Zhu J X, Si Q, Minár J, Yan B and Yi M 2024 *Nat. Commun.* **15** 9376

[119] Zhang H, Oli B D, Zou Q, Guo X, Wang Z and Li L 2023 *Nat. Commun.* **14** 6167

[120] Sales B C, Meier W R, May A F, Xing J, Yan J Q, Gao S, Liu Y H, Stone M B, Christianson A D, Zhang Q and McGuire M A 2021 *Phys. Rev. Mater.* **5** 044202

[121] Huang L and Lu H 2020 *Phys. Rev. B* **102** 125130

[122] Lin Z, Choi J H, Zhang Q, Qin W, Yi S, Wang P, Li L, Wang Y, Zhang H, Sun Z, Wei L, Zhang S, Guo T, Lu Q, Cho J H, Zeng C and Zhang Z 2018 *Phys. Rev. Lett.* **121** 096401

[123] Hou Z, Ren W, Ding B, Xu G, Wang Y, Yang B, Zhang Q, Zhang Y, Liu E, Xu F, Wang W, Wu G, Zhang X, Shen B and Zhang Z 2017 *Adv. Mater.* **29** 1701144

[124] Li M, Wang Q, Zhou L, Song W, Ma H, Ding P, Fedorov A, Huang Y, Büchner B, Lei H, Wang S and Lou R 2024 *Chin. Phys. B* **33** 117101

[125] Venturini G, Idrissi B C E and Malaman B 1991 *J. Magn. Magn. Mater.* **94** 35

[126] Venturini G, Welter R, Malaman B and Ressouche E 1993 *J. Alloys Compd.* **200** 51

[127] Venturini G, Fruchart D and Malaman B 1996 *J. Alloys Compd.* **236** 102

[128] Ghimire N J, Dally R L, Poudel L, Jones D C, Michel D, Magar N T, Bleuel M, McGuire M A, Jiang J S, Mitchell J F, Lynn J W and Mazin I I 2020 *Sci. Adv.* **6** eabe2680

[129] Chen D, Le C, Fu C, Lin H, Schnelle W, Sun Y and Felser C 2021 *Phys. Rev. B* **103** 144410

[130] Ma W, Xu X, Yin J X, Yang H, Zhou H, Cheng Z J, Huang Y, Qu Z, Wang F, Hasan M Z and Jia S 2021 *Phys. Rev. Lett.* **126** 246602

[131] Chafik El Idrissi B, Venturini G, Malaman B and Ressouche E 1994 *J. Alloys Compd.* **215** 187

[132] Venturini G, Welter R and Malaman B 1992 *J. Alloys Compd.* **185** 99

[133] Rao X L and Coey J M D 1997 *J. Appl. Phys.* **81** 5181

[134] Mazet T and Malaman B 2001 *J. Alloys Compd.* **325** 67

[135] Peng S, Han Y, Pokharel G, Shen J, Li Z, Hashimoto M, Lu D, Ortiz B R, Luo Y, Li H, Guo M, Wang B, Cui S, Sun Z, Qiao Z, Wilson S and He J 2021 *Phys. Rev. Lett.* **127** 266401

[136] Hu Y, Wu X, Yang Y, Gao S, Plumb N C, Schnyder A P, Xie W, Ma J and Shi M 2022 *Sci. Adv.* **8** eadd2024

[137] Pokharel G, Teicher S M L, Ortiz B R, Sarte P M, Wu G, Peng S, He J, Seshadri R and Wilson S D 2021 *Phys. Rev. B* **104** 235139

[138] Arachchige H W S, Meier W R, Marshall M, Matsuoka T, Xue R, McGuire M A, Hermann R P, Cao H and Mandrus D 2022 *Phys. Rev. Lett.* **129** 216402

[139] Hu Y, Teicher S M L, Ortiz B R, Luo Y, Peng S, Huai L, Ma J, Plumb N C, Wilson S D, He J and Shi M 2022 *Science Bulletin* **67** 495

[140] Cho S, Ma H, Xia W, Yang Y, Liu Z, Huang Z, Jiang Z, Lu X, Liu J, Liu Z, Li J, Wang J, Liu Y, Jia J, Guo Y, Liu J and Shen D 2021 *Phys. Rev. Lett.* **127** 236401

[141] Zhao Z, Yao J, Xu R, Wang Y, Liao S, Liu Z, Shen D, Cui S, Sun Z, Wang Y, Feng D and Jiang J 2024 *Chin. Phys. B* **33** 107403

[142] Huai L, Luo Y, Teicher S M L, Ortiz B R, Wang K, Peng S, Wei Z, Shen J, Wang B, Miao Y, Sun X, Ou Z, Wilson S D and He J 2022 *Chin. Phys. B* **31** 057403

[143] Xu Y, Ni Z, Liu Y, Ortiz B R, Deng Q, Wilson S D, Yan B, Balents L and Wu L 2022 *Nat. Phys.* **18** 1470

[144] Liu B, Kuang M Q, Luo Y, Li Y, Hu C, Liu J, Xiao Q, Zheng X, Huai L, Peng S, Wei Z, Shen J, Wang B, Miao Y, Sun X, Ou Z, Cui S, Sun Z, Hashimoto M, Lu D, Jozwiak C, Bostwick A, Rotenberg E, Moreschini L, Lanzara A, Wang Y, Peng Y, Yao Y, Wang Z and He J 2023 *Phys. Rev. Lett.* **131** 026701

[145] Li Y, Liu Y, Du X, Wu S, Zhao W, Zhai K, Hu Y, Zhang S, Chen H, Liu J, Yang Y, Peng C, Hashimoto M, Lu D, Liu Z, Wang Y, Chen Y, Cao G and Yang L 2024 arXiv:2406.03740 [cond-mat.str-el]

[146] Guo Y, Wang Z, Xie F, Huang Y, Gao B, Oh J S, Wu H, Liu Z, Ren Z, Fang Y, Biswas A, Zhang Y, Yue Z, Hu C, Jozwiak C, Bostwick A, Rotenberg E, Hashimoto M, Lu D, Kono J, Chu J H, Yakobson B I, Birgeneau R J, Si Q, Dai P and Yi M 2024 arXiv:2406.05293 [cond-mat.str-el]

[147] Peng S, Han Y, Li Y, Shen J, Miao Y, Luo Y, Huai L, Ou Z, Li H, Xiang Z, Liu Z, Shen D, Hashimoto M, Lu D, Yao Y, Qiao Z, Wang Z and He J 2024 arXiv:2406.17769 [cond-mat.supr-con]

[148] Liu Y, Liu Z Y, Bao J K, Yang P T, Ji L W, Wu S Q, Shen Q X, Luo J, Yang J, Liu J Y, Xu C C, Yang W Z, Chai W L, Lu J Y, Liu C C, Wang B S, Jiang H, Tao Q, Ren Z, Xu X F, Cao C, Xu Z A, Zhou R, Cheng J G and Cao G H 2024 *Nature* **632** 1032

[149] Shi M, Yu F, Yang Y, Meng F, Lei B, Luo Y, Sun Z, He J, Wang R, Jiang Z, Liu Z, Shen D, Wu T, Wang Z, Xiang Z, Ying J and Chen X 2022 *Nat. Commun.* **13** 2773

[150] Hu Y, Le C, Chen L, Deng H, Zhou Y, Plumb N C, Radovic M, Thomale R, Schnyder A P, Yin J X, Wang G, Wu X and Shi M 2024 *Phys. Rev. B* **110** L121114

[151] Pradhan Sakhya A, Ortiz B R, Ghosh B, Sprague M, Islam Mondal M, Matzelle M, Elius I B, Valadez N, Mandrus D G, Bansil A and Neupane M 2023 arXiv:2309.01176 [cond-mat.mes-hall]

[152] Zheng Z, Chen L, Ji X, Zhou Y, Qu G, Hu M, Huang Y, Weng H, Qian T and Wang G 2024 *Science China Physics, Mechanics & Astronomy* **67** 267411

[153] Jiang Z, Li T, Yuan J, Liu Z, Cao Z, Cho S, Shu M, Yang Y, Ding J, Li Z, Liu J, Liu Z, Liu J, Ma J, Sun Z, Guo Y and Shen D 2023 arXiv:2309.01579 [cond-mat.str-el]

[154] Ortiz B R, Miao H, Parker D S, Yang F, Samolyuk G D, Clements E M, Rajapitamahuni A, Yilmaz T, Vescovo E, Yan J, May A F and McGuire M A 2023 *Chemistry of Materials* **35** 9756

[155] Li S, Zeng B, Wan X, Tao J, Han F, Yang H, Wang Z and Wen H H 2011 *Phys. Rev. B* **84** 214527

[156] Gong C, Tian S, Tu Z, Yin Q, Fu Y, Luo R and Lei H 2022 *Chin. Phys. Lett.* **39** 087401

[157] Yin J X, Zhang S S, Chang G, Wang Q, Tsirkin S S, Guguchia Z, Lian B, Zhou H, Jiang K, Belopolski I, Shumiya N, Multer D, Litskevich M, Cochran T A, Lin H, Wang Z, Neupert T, Jia S, Lei H and Hasan M Z 2019 *Nat. Phys.* **15** 443

[158] Xu Y, Zhao J, Yi C, Wang Q, Yin Q, Wang Y, Hu X, Wang L, Liu E, Xu G, Lu L, Soluyanov A A, Lei H, Shi Y, Luo J and Chen Z G 2020 *Nat. Commun.* **11** 3985

[159] Morali N, Batabyal R, Nag P K, Liu E, Xu Q, Sun Y, Yan B, Felser C, Avraham N and Beidenkopf H 2019 *Science* **365** 1286

[160] Mielke Iii C, Liu H, Das D, Yin J X, Deng L Z, Spring J, Gupta R, Medarde M, Chu C W, Khasanov R, Hasan Z M, Shi Y, Luetkens H and Guguchia Z 2022 *J. Phys.: Condens. Matter* **34** 485601

[161] Roy S B and Chaddah P 1999 *Pramana J. Phys.* **53** 659